

# The Cosmological Signatures and Flux Distribution of Gamma-Ray Bursts with a Broad Luminosity Distribution<sup>1</sup>

J. J. Brainerd<sup>2</sup>

University of Alabama in Huntsville

## ABSTRACT

The cosmological expansion cannot produce the reported correlations of the gamma-ray burst timescale and spectral energy with peak flux if the burst model reproduces the BATSE 3B peak-flux distribution for a non-evolving burst source density. The required ratios of time dilation and redshift factors are only produced by monoluminous models at peak fluxes below the BATSE threshold, and they are never produced by power-law luminosity models. Monoluminous models only produce acceptable fits to the peak-flux distribution for very specific combinations of the spectral and cosmological parameters. The redshift of gamma-ray bursts at the BATSE threshold is  $z \approx 1.5$ . Power law luminosity distribution models  $\propto L^{-\beta}$  produce acceptable fits to the data for most values of the spectral parameters when  $\beta < 1.6$ . In this model, gamma-ray bursts of a given peak flux have a distribution of redshifts, with a maximum redshift of  $\gtrsim 3$  for peak fluxes near the BATSE threshold, and with an average redshift of  $< 1$  for all values of peak flux. This qualitative behavior occurs whenever the luminosity distribution determines the shape of the peak-flux distribution, regardless of whether source density evolution occurs. The reported correlations of the burst timescale and the spectral energy with peak flux are systematically 1 standard deviation above the monoluminous model and 1.5 to 2 standard deviation above the power-law luminosity model. These results suggest that an intrinsic correlation of burst timescale and spectral energy with luminosity is present. Studies of the peak-flux distribution for bursts selected by  $E_{peak}$  or hardness ratio provide a test for this intrinsic correlation.

*Subject headings:* Gamma rays: bursts

---

<sup>1</sup>To appear in The Astrophysical Journal, Sept. 20, 1997

<sup>2</sup>e-mail: jim.brainerd@msfc.nasa.gov

## 1. The Indistinctness of Cosmological Signatures

Gamma-ray bursts are widely believed to be cosmological, but no direct measurement of distance exists to confirm this belief. No gamma-ray burst has lines that can be associated with atomic or nuclear processes, so a direct calculation of their redshifts is not possible. With only one recent exception (Groot et al. 1997), no gamma-ray burst has an observed counterpart, so an indirect calculation of their redshifts is also not possible. Because of these difficulties, a number of researchers have attempted to derive average redshifts by studying the properties of gamma-ray burst catalogs. The simplest of these studies fit the peak-flux distribution to cosmological models under various assumptions (e.g. Fenimore et al. 1993; Wickramasinghe et al. 1993; Emslie & Horack 1994; Cohen & Piran 1995; Pendleton et al. 1996; Petrosian & Lee 1997). More involved studies attempt to measure a correlation of gamma-ray burst timescale with photon flux under the assumption that such a correlation is evidence of a cosmological time dilation (Norris et al. 1994; Davis et al. 1994; Mitrofanov et al. 1994, 1996; Lee & Petrosian 1996). Related studies attempt to measure a correlation of the characteristic photon energy with flux, which may indicate a cosmological redshift (Nemiroff et al. 1994; Mallozzi et al. 1995).

The difficulty with these approaches is that the interpretation of the results is not unique. The observed flux distribution simply shows that gamma-ray bursts are not homogeneously distributed in space, which is unique neither to a cosmological origin nor to a particular model of cosmological expansion. Galactic corona models of gamma-ray bursts easily reproduce the observations (Brainerd 1992; Ulmer & Wijers 1995; Ulmer et al. 1995; Hakkila et al. 1995), and any cosmological model can be made to conform to the observations with the proper choice of density evolution (Rutledge et al. 1995; Horack et al. 1995; Reichart & Mészáros 1997), or luminosity distribution (Mészáros & Mészáros 1995; Hakkila et al. 1996), as is evident from the numerous combinations of assumptions made by the numerous papers examining this topic. The effects sought in correlation studies can be explained by an intrinsic correlation of the parameter of interest with the luminosity (Brainerd 1994a). The beaming of relativistic jets (Brainerd 1994a; Yi 1994) and the conservation of total energy in monoenergetic sources (Wijers & Paczyński 1994) are examples of mechanisms that produce such a correlation.

The question addressed in this article is whether a strong correlation of the burst time scale or the characteristic spectral energy with peak flux can have a purely cosmological origin when the gamma-ray burst peak-flux distribution is determined by the luminosity distribution rather than by the spatial distribution. In this study, I use a luminosity function that is a power law with an upper limit, and, for comparison, a monoluminous distribution. The spectral model I use (§2) is the Compton attenuation model (Brainerd

1994b), which accurately represents the observed spectra. The cosmological expansion with a  $(1+z)^\mu$  comoving source density ( $\mu < 9/2$ ) defines a limiting power-law index for the peak flux distribution that is  $> -5/2$  as the peak flux goes to zero; a luminosity distribution can drive this index closer to  $-5/2$  (§3 and §4). When the luminosity function determines the asymptotic behavior of the peak flux distribution, the density evolution of the gamma-ray burst sources has only a weak effect on the average time-dilation and redshift (§3). I find (§5) that a broad luminosity distribution in a Friedmann cosmology with a constant comoving source density produces peak-flux distributions that fit well the distribution observed by the Burst and Transient Source Experiment (BATSE) on the Compton Gamma-Ray Observatory. At a given flux, the gamma-ray bursts have a redshift distribution, with the average redshift considerably smaller than the maximum redshift (§4). The maximum redshift a burst can have at the BATSE threshold is  $\gtrsim 3$ . In this model, the cosmological expansion cannot explain the reported correlations (§6), so an intrinsic correlation must exist. The flux distribution for gamma-ray bursts selected by hardness ratio presented in recent studies is a measure of this intrinsic correlation (§7). These studies offer the opportunity to separate the cosmological effects from the intrinsic correlations.

## 2. Spectral Parameterization

Gamma-ray burst spectra are not power-law spectra; they are hard spectra that gradually roll over in the 50 keV to 300 keV energy band to a power law, with the power-law behavior appearing above 1 MeV (Metzger et al. 1974; Hueter 1984; Matz et al. 1985). The choice of spectral model influences the shape of the burst peak-flux distribution (Brainerd 1994b; Mallozzi et al. 1996). A physical spectral model that accurately describes gamma-ray burst spectra is a Compton-attenuated power-law spectrum (Brainerd 1994b; Brainerd et al. 1996a,b). Because this spectrum is a testable gamma-ray burst theory, it is of interest beyond its descriptive value.

This spectrum is defined by four parameters in the gamma-ray energy band: a Thomson optical depth  $\tau_T$ , a parameter  $\Psi \equiv (\delta + 2)/\tau_T < 0$ , where  $\delta$  is the power-law index of the spectrum as  $\nu \rightarrow \infty$ , a redshift  $z$ , and an overall normalization. In the discussion that follows, the spectral parameter  $z$  is set to 0, so that the cosmological redshift enters explicitly through equation (7). The overall normalization is folded into the free parameter  $L$ , which is a luminosity that is defined in equation (6). The two remaining parameters describe the shape of the spectrum. The parameter  $\Psi$  sets the peak energy  $E_p$  of  $\nu F_\nu$  in the cosmological comoving frame, and the parameter  $\tau_T$  defines the width of  $\nu F_\nu$  about  $E_p$ . The energy  $E_p$  only exists for  $\Psi > -0.1972$ , taking on a minimum

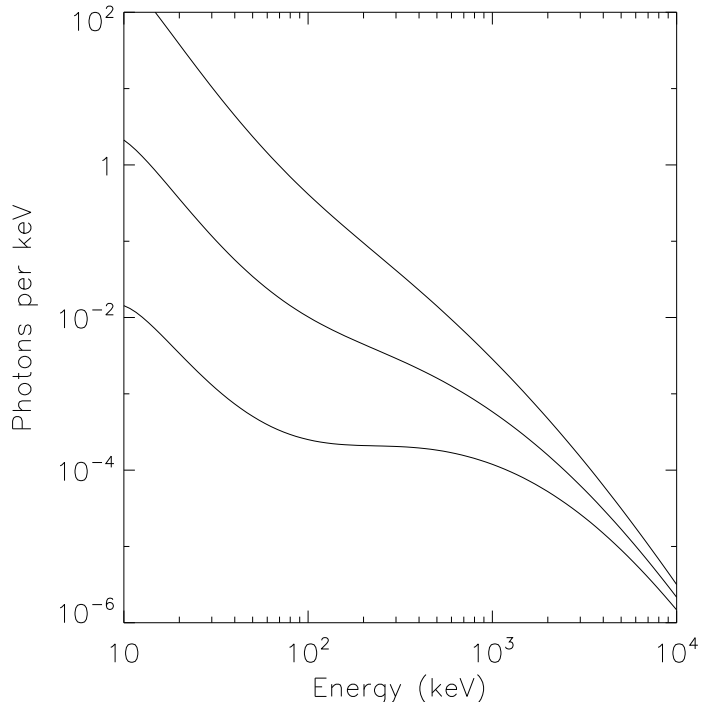


**Fig. 1**—Compton attenuated spectrum. For all three curves, the spectral parameter  $\delta = -4$ . From top to bottom, the curves have  $\tau_T = 10, 15,$  and  $20$ , corresponding to  $\Psi = -0.20, -0.13,$  and  $-0.10$  respectively.

value of 231 keV at  $\Psi = -0.1972$ . For  $0 < -\Psi \ll 0.1972$ , the value of  $E_p$  is given by  $\Psi = -\log(2E_p/m_e c^2) m_e c^2/E_p$ , so a wide range of  $\Psi$  values produces a narrow range of  $E_p$  values. The width in  $\log E$  of the  $\nu F_\nu$  curve about  $E_p$  is proportional to  $1/\sqrt{\tau_T}$ . General values of these parameters that produce good fits to the data are  $10 \lesssim \tau_T \lesssim 30$  and  $-0.16 < \Psi < -0.12$  (Brainerd et al. 1996b). Three examples are given in Figure 1. In this figure,  $\delta = -4$  and  $\tau_T = 10, 15,$  and  $20$ , which gives  $\Psi = -0.20, -0.133,$  and  $-0.10$  respectively; the uppermost curve does not have an  $E_p$  since  $\Psi < -0.1972$ . The inflection point at 231 keV is apparent in these spectra. The x-ray upturn predicted by this spectrum has been observed (Preece et al. 1996; Brainerd et al. 1996a,b). In this study, only the spectrum above 50 keV is used.

### 3. The General Gamma-Ray Burst Flux Distribution

The equation for the flux distribution of cosmological gamma-ray bursts is well known. The general equations for the number of gamma-ray bursts per unit proper time  $\tau$  per unit proper volume  $V$  per unit luminosity  $L$  per unit spectral parameter space  $\vec{p}$  is

$$\frac{dN}{d\tau dV dL d^n p} = \rho(\tau, r, L, \vec{p}) = R(\tau)^{-3} n_0(\tau) \Phi(L, \vec{p}), \quad (1)$$

where the second equality expresses the assumption that the characteristics of a gamma-ray burst are independent of the age of the universe. The function  $n_0(\tau)$  is the number of gamma-ray bursts per unit proper time per unit comoving volume. The function  $\Phi(L, \vec{p})$  is the fraction of gamma-ray bursts per unit luminosity per unit spectral parameter space; it is normalized to unity. The proper time of the gamma-ray burst source is related to the observer's time by

$$dt = (1 + z) d\tau, \quad (2)$$

and the volume element is related to the coordinate elements through

$$dV = R(\tau)^3 \frac{r^2}{\sqrt{1 - (2q_0 - 1)r^2}} dr d\Omega, \quad (3)$$

where the nonstandard coordinate radius  $r$  is defined in terms of the Robertson-Walker coordinate radius  $r_1$  as  $r = r_1 H_0 R_0 / c$ . The parameter  $R(\tau)$  is  $c/H_0 R_0$  times the expansion parameter for the Robertson-Walker metric, and the factor  $\sqrt{1 - (2q_0 - 1)r^2}$  in equation (3) is the familiar  $\sqrt{1 - kr_1^2}$  from the Robertson-Walker metric. The coordinate radius is related to the redshift by

$$r = \frac{q_0 z + (q_0 - 1)(\sqrt{1 + 2q_0 z} - 1)}{q_0^2 (1 + z)} = \frac{2z(1 + z + \sqrt{1 + 2q_0 z})}{(1 + z)(1 + \sqrt{1 + 2q_0 z})^2}. \quad (4)$$

From the formal derivation of equation (4) (Weinberg 1972, eq. [15.3.23]), the first derivative of  $r$  with  $z$  is

$$\frac{dr}{dz} = \frac{\sqrt{1 - (2q_0 - 1)r^2}}{\sqrt{1 + 2q_0 z} (1 + z)}. \quad (5)$$

The gamma-ray number flux  $F$  in an energy band spanning the frequencies  $\nu_1$  to  $\nu_2$  is related to the luminosity by

$$F = \frac{L H_0^2}{c^2} \mathcal{F}(z, \vec{p}), \quad (6)$$

where the length scale  $R_0$  is folded into the luminosity  $L$ , and the function  $\mathcal{F}(z, \vec{p})$ , which is defined as

$$\mathcal{F}(z, \vec{p}) = r^{-2} \int_{\nu_1}^{\nu_2} I[\nu(1 + z), \vec{p}] d\nu, \quad (7)$$

is the photon number flux normalized by the overall luminosity. The function  $I(\nu)$  is the photon number flux per unit frequency. The purpose of this particular parameterization is to separate the luminosity  $L$  from the spectral shape parameters  $\vec{p}$ .

With equations (2) through (7), one can transform equation (1) into a distribution over observable parameters:

$$\frac{dN}{dt d\Omega dF dz d^n p} = n_0 [\tau(z)] \Phi\left(\frac{F}{\mathcal{F}(z)}, \vec{p}\right) \mathcal{F}(z)^{-1} \frac{r^2}{(1+z)^2 \sqrt{1+2q_0 z}}. \quad (8)$$

This equation differs from the equation for galaxy distributions by a factor of  $1/(1+z)$ , which arises from the time dilation of the burst rate.

The distribution of bursts with flux is given by the integration of equation (8) over all  $z$ . For this integral to be bounded,  $\Phi(L, \vec{p})$  must have limits on its asymptotic behavior as  $L \rightarrow 0$  and  $L \rightarrow \infty$ . If we assume that  $\Phi(L, \vec{p}) \propto L^{-\beta_l}$  for  $L \ll L_0$ , where  $L_0$  characterizes the peak of the function  $L^{5/2} \Phi(L, \vec{p})$ , then the integral of equation (8) over  $z$  converges as  $z \rightarrow 0$  when  $\beta_l < 5/2$ . If  $\Phi(L, \vec{p}) \propto L^{-\beta_h}$  for  $L \gg L_0$ , the integral converges as  $z \rightarrow \infty$  when  $\beta_h > 5/2$ . While the second limit is derived under the assumption that  $z \ll 1$  when  $L \gg L_0$ , relaxing this assumption lowers the value on the right side of the inequality, so the condition holds for all parameter space.

### 3.1. Asymptotic Behavior

The flux appears in equation (8) only in the argument of the luminosity distribution function. The asymptotic behavior with flux of the integral of equation (8) over  $z$  is therefore determined by the behavior of  $\Phi(L, \vec{p})$  at the values of  $z$  producing the greatest contribution to the integral. If this occurs for values of  $z$  that give  $L \approx L_0$ , then the integration variable  $z$  can be replaced by  $L$ , and the expansion of factors involving  $z$  determine the asymptotic behavior with  $F$ . On the other hand, if the integrand peaks at values of  $z$  such that  $L \ll L_0$  or  $L \gg L_0$ , then it is the asymptotic behavior of  $\Phi(L, \vec{p})$  that determines the asymptotic behavior of the flux distribution with  $F$ .

When  $z \ll 1$  for  $L \gg L_0$ , the flux is  $\propto L/z^2$ , and equation (8) is  $\propto \Phi(L, \vec{p}) z^4$ , assuming no density evolution at  $z \ll 1$ . The integrand peaks at  $L_0$ , so its contribution to the integral above  $z \approx 1$  is negligible. Integrating over  $z$  and changing the variable of integration to  $L$  then gives the flux distribution, which is proportional to  $F^{-5/2}$ . This is the origin of the  $-3/2$  slope of the  $\log N$ - $\log F$  curve of a homogeneous distribution.

Of more interest is the behavior of equation (8) when  $z \gg 1$  for  $L \approx L_0$ . To discuss the asymptotic behavior of the integral in this regime, I let the photon spectrum be a power law, so that  $I_\nu \propto \nu^\delta$ , with  $\delta < -2$ . This is justified by the observed power-law behavior above 1 MeV. I also assume that  $\Phi(L, \vec{p}) \propto L^{-\beta}$  when  $L \gg L_0$  or  $L \ll L_0$ , with  $\beta = \beta_h$  for the first condition and  $\beta = \beta_l$  for the second. Finally, I set  $n_0(\tau) \propto (1+z)^\mu$  to investigate

the effects of density evolution. A necessary and sufficient condition for the integral over equation (8) to be bounded under these assumptions is that  $\beta_l < 5/2$ , which guarantees the convergence of the integral as  $z \rightarrow 0$ , and  $\beta_h > 1 + (3/2 - \mu)/\delta$ , which guarantees convergence as  $z \rightarrow \infty$ . Because  $\beta_h > 5/2$  is already required for convergence in the regime of  $z_0 \ll 1$ , this last criterion is satisfied when  $\mu < 3(1 - \delta)/2$ . Because  $\delta < -2$ , the right side of this inequality is  $> 9/2$ , so this second condition on  $\beta_h$  is only important for very strong evolution. I assume that this limit on  $\mu$  holds in the discussion below.

When  $z \gg 1$  for  $L \approx L_0$ , the integral can be divided into four parts that are bounded by  $z = 1$ ,  $z = 1/q_0 > 1$ , and  $L(z) = L_0$ . When the integral peaks at a value  $z_0$  that is either of these first two values, the factor of  $F$  in the argument of the luminosity function can be factored out of the integral. The distribution in flux is then proportional to  $F^{-\beta}$ . There remains two questions to answer: when is  $z_0$  at  $L(z_0) \approx L_0$ , and what is the dependence on  $F$  of the flux distribution in this case?

Two regimes exist that affect the dependence of the burst distribution when  $L(z_0) \approx L_0$ :  $1 < z_0 < 1/q_0$  and  $z_0 > 1/q_0$ . In the first regime, equation (8) has the asymptotic integral form of

$$\frac{dN}{dt d\Omega dF d^n p} = n_c \int_0^\infty \Phi\left(\frac{F}{\mathcal{F}(z)}, \vec{p}\right) \mathcal{F}(z)^{-1} z^\mu dz. \quad (9)$$

Because  $\mathcal{F}(z) \propto z^{-2-\delta}$  in this regime (eq. [7] and [4]), this equation becomes

$$\frac{dN}{dt d\Omega dF d^n p} \propto F^{-1-\frac{1+\mu}{2-\delta}}. \quad (10)$$

Necessary and sufficient conditions for  $L(z_0) \approx L_0$  are  $\beta_l < 1 + \frac{1+\mu}{2-\delta}$  and  $\beta_h > 1 + \frac{1+\mu}{2-\delta}$ . Because I am assuming  $\mu < 9/2$  and  $\delta < -2$ , the strongest condition on  $\beta_h$  is  $\beta_h > 19/11$ , which is weaker than the earlier condition of  $\beta_h > 5/2$ . As a consequence, one never can have  $z_0 \approx 1/q_0$ . The only possibility is to violate the condition on  $\beta_l$ , in which case  $z_0 \approx 1$  in the  $1 < z_0 < 1/q_0$  regime. Because of this, the general asymptotic equations for the burst flux distribution is

$$\frac{dN}{dt d\Omega dF d^n p} \propto F^{-\alpha_1}, \quad (11)$$

where

$$\alpha_1 = \max\left(\beta_l, 1 + \frac{1+\mu}{2-\delta}\right). \quad (12)$$

In the second regime, where  $z_0 > 1/q_0$ , the asymptotic form of the integral over equation (8) is

$$\frac{dN}{dt d\Omega dF d^n p} = n_c \int_0^\infty \Phi\left(\frac{F}{\mathcal{F}(z)}, \vec{p}\right) \mathcal{F}(z)^{-1} z^{\mu-\frac{5}{2}} dz. \quad (13)$$

In this regime,  $\mathcal{F}(z) \propto z^\delta$ , so the dependence of the flux distribution on  $F$  is

$$\frac{dN}{dt d\Omega dF d^n p} \propto F^{-1+\frac{\mu-3/2}{\delta}}. \quad (14)$$

Sufficient (but not necessary) conditions for  $L(z_0) \approx L_0$  are  $\beta_l < 1 + \frac{1+\mu}{2-\delta}$ ,  $\beta_l < 1 - \frac{\mu-3/2}{\delta}$ , and  $\mu > (6 - 5\delta)/4$ . The last condition guarantees that the integration does not have secondary maximum at  $z = 1$ . Because I assume  $\delta < -2$  and  $\mu < 9/2$ , this last condition is always satisfied. As a consequence, the second condition on  $\beta_l$  is the stronger, and the general asymptotic solution can be written as

$$\frac{dN}{dt d\Omega dF d^n p} \propto F^{-\alpha_2}, \quad (15)$$

where

$$\alpha_2 = \max\left(\beta_l, 1 - \frac{\mu - \frac{3}{2}}{\delta}\right). \quad (16)$$

Several points are immediately clear from these equations. First, the behavior of the luminosity distribution function below  $L_0$  influences the asymptotic behavior of the flux distribution, while the behavior above  $L_0$  is unimportant. Recall that  $L_0$  is defined as the maximum of  $L^{5/2}\Phi(L, \vec{p})$ . Second, in the absence of strong source evolution, a large asymptotic power-law index at small  $F$  requires a luminosity distribution with a power-law index of equal value, as noted by Mészáros & Mészáros (1995). Because  $\delta < -2$ , the minimum value of  $\alpha_1$ , which is given by the second term in equation (12), is  $< 5/4$  for  $\mu = 0$ ; from the second term of equation (16), the minimum value of  $\alpha_2$  is  $< 1/4$  for  $\mu = 0$ . Third, because the luminosity function can formally diverge and still give a bounded integral as long as it falls below a  $L^{-5/2}$  power law as  $L \rightarrow 0$ , the presence of a change in the luminosity distribution function at sufficiently low luminosity—which is required by the boundedness of  $\int \Phi(L) dL$ —has no effect on the observed flux distribution; formally, this must be at  $L \ll F_{min}c^2/H_0^2\mathcal{F}(1)$ , where  $F_{min}$  is the minimum observable burst flux (Mészáros & Mészáros 1995). Finally, evolution is unimportant in the asymptotic behavior unless the number of bursts increases dramatically as  $1+z$  increases; the second index in equation (12) increases by  $< \mu/4$ , and the second index in equation (16) increases by  $< \mu/2$ , so evolution cannot dominate the luminosity distribution function unless  $\mu \gtrsim 3$ .

Equations (12) and (16) imply different behaviors for  $q_0 = 0.5$  and  $q_0 \ll 0.5$ . For  $q_0 = 0.5$ , the only relevant limit is that given by equation (16). When  $z_0 \ll 1$ , the integrand rises with  $z$  until the peak in  $\Phi(L, \vec{p})$  is reached. When  $z_0 \gg 1$ , the integrand rises until  $z \approx 1$ ; then, if  $\beta_l > 1 - (\mu - \frac{3}{2})/\delta$ , the integrand goes to zero more rapidly than  $z^{-1}$  as  $z \rightarrow \infty$ , but if the inequality is violated, the integrand either rises or goes to zero less



rapidly than  $z^{-1}$ . In contrast, when  $q_0 \ll 0.5$ , there are three regimes to consider. As in the previous case, when  $z_0 < 1$ , the integrand rises to the maximum of  $\Phi(L, \vec{p})$ , but for  $1 < z_0 < 1/q_0$ , equation (12) applies, and the integrand goes to zero more rapidly than  $z^{-1}$  when  $\beta_l > 1 + (1 + \mu) / (2 - \delta)$ , and rises or goes to zero less rapidly than  $z^{-1}$  when the inequality does not hold. When  $z_0 > 1/q_0$ , equation (16) holds, and the behavior noted for  $q_0 = 0.5$  holds for  $q_0 \ll 0.5$ . The consequences of this behavior are that the minimum value of  $\alpha$  in an  $F^{-\alpha}$  asymptotic description of the flux distribution is strongly dependent on  $q_0$  and that, for  $q_0 \ll 0.5$ , the distribution in  $z$  for bursts with a given  $F$  is broad and flat over  $1 < z_0 < 1/q_0$  when  $1 + (1 + \mu) / (2 - \delta) > \beta_l > 1 - (\mu - \frac{3}{2}) / \delta$ .

#### 4. Incorporating a Luminosity Distribution

The gamma-ray burst flux distribution is derived for two luminosity distributions: a monoluminous distribution function, and a power-law luminosity distribution with a high luminosity cutoff. The first is widely used, and it is given here for comparison to the power law distribution.

##### 4.1. Monoluminous Distribution

The equation for a monoluminous gamma-ray burst distribution does not have an integral over  $z$ . It is therefore relatively easy to evaluate and fit to the observed flux distribution. From equations (1) through (6),

$$\frac{dN}{dF} = N_0 \frac{4r^2 \sqrt{1 + 2q_0}}{(1 + z)^2 r_0^2 \sqrt{1 + 2q_0} z} \left[ \frac{d\mathcal{F}(z)/dz|_{z=1}}{d\mathcal{F}(z)/dz} \right]. \quad (17)$$

In this equation,  $r_0$  is the value of  $r$  from equation (4) for  $z = 1$ . The normalization  $N_0$  is the number of bursts per unit  $F$  at  $z = 1$ .  $F$  is related to  $z$  through

$$F = F_0 \frac{\mathcal{F}(z)}{\mathcal{F}(1)}, \quad (18)$$

where  $\mathcal{F}(z)$  is given by equation (7).

The distributions produced by equation (17) are plotted as dotted lines in Figure 2 for  $F_0 = 1$ ,  $N_0 = 1$ ,  $\Psi = -0.15$ , and  $\tau_T = 15$  for both  $q_0 = 0.5$  and  $0.1$ . The curves for  $z$  given by equation (18) as a function of  $F$  are plotted in Figure 4 for these parameters. The curves in Figure 2 go to the correct limiting power-law indices: for  $q_0 = 0.5$ , it is given by equation (16) as  $11/17$  ( $\approx 0.65$ ), while for  $q_0 = 0.1$ , it is given by equation (12) as  $29/25$  ( $\approx 1.16$ ).

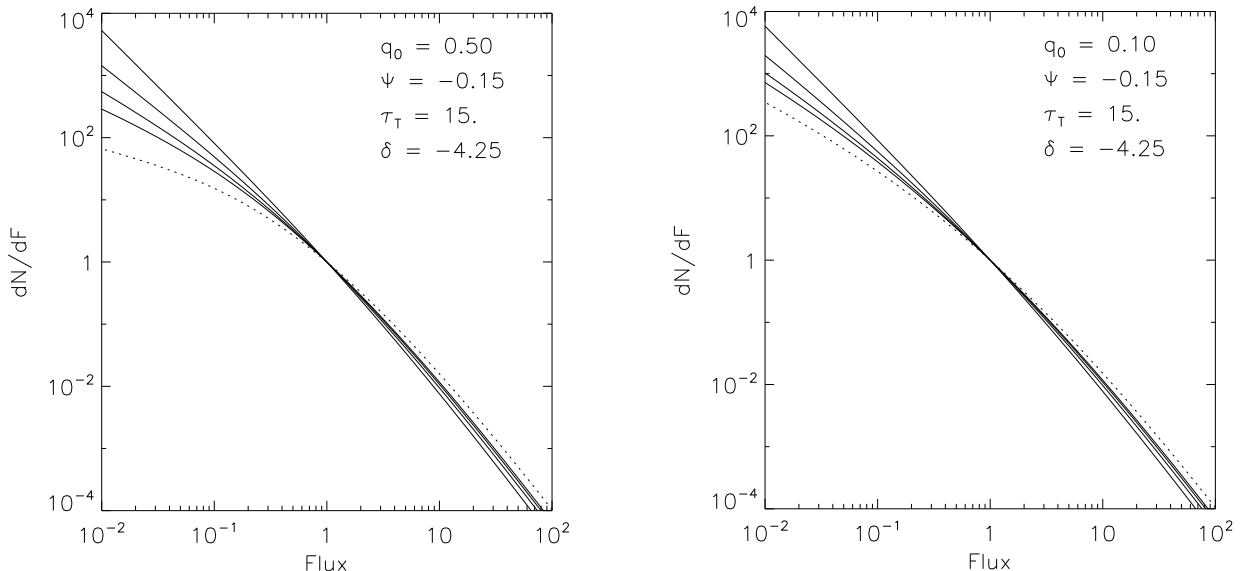


**Fig. 2**—Peak-flux distributions. All curves are for spectral parameters  $\Psi = -0.15$  and  $\tau_T = 15$ , which are defined in §2. The figures are for  $q_0 = 0.5$  (left) and 0.1 (right). The solid curves for a power-law luminosity distributions with (top left to bottom left)  $\beta = 1.8, 1.4, 1.0,$  and 0.6. The solid curve is the monoluminosity distribution for the given spectral and cosmological parameters. The curves are normalized by  $N_0 = 1$  and  $F_0 = 1$  so that  $dN/dF = 1$  and  $z_{max} = 1$  at  $F = 1$ . The flux is measured in the 50 keV to 300 keV energy band.

## 4.2. Cutoff Power-Law Luminosity Distribution

A simple distribution function used frequently in gamma-ray burst studies is a power-law distribution with one or two luminosity cutoffs. In this study, I use

$$\Phi(L) = \begin{cases} \left(\frac{L}{L_0}\right)^{-\beta}, & \text{for } L \leq L_0; \\ 0, & \text{otherwise.} \end{cases} \quad (19)$$

Placing this into equation (8) and integrating over  $z$  gives

$$\frac{dN}{dF} = n_0 \left(\frac{F}{F_0}\right)^{-\beta} \int_0^{z_{max}} \mathcal{F}^{\beta-1}(z) \frac{r^2}{(1+z)^2 \sqrt{1+2q_0z}} dz, \quad (20)$$

where  $z_{max}$  is defined for a given flux  $F$  by equation (18) with  $z$  replaced by  $z_{max}$ . The normalizing flux  $F_0$  is the flux at which  $z_{max} = 1$ . The normalization parameter  $n_0$  is

defined as

$$n_0 = N_0 / \int_0^1 \mathcal{F}^{\beta-1}(z) \frac{r^2}{(1+z)^2 \sqrt{1+2q_0z}} dz, \quad (21)$$

where  $N_0$  is the number of gamma-ray bursts per unit flux at  $F = F_0$ .

Flux distributions from equation (20) with  $F_0 = 1$  and  $N_0 = 1$  are plotted in Figure 2 as solid lines for  $\beta = 0.6, 1.0, 1.4,$  and  $1.8$  for both  $q_0 = 0.5$  and  $0.1$ . The asymptotic behavior discussed in §3.1 is clearly demonstrated in these figures. For  $q_0 = 0.5$ , equation (16) states that the asymptotic power-law index is given by  $-\beta$  when  $\beta > 11/17 \approx 0.65$ . Three of the four solid curves in this plot satisfy this criterion, and all three are close to their asymptotic values at low flux. The fourth, which has  $\beta = 0.6$ , is slowly going to the asymptotic value of  $-\beta = -11/17$ . For  $q_0 = 0.1$ , the limit on  $\beta$  is given by equation (12), because  $z_{max} > 6$  for the fluxes in the plot, and equation (16) is not applicable until  $z_0 \gg 10$ . In this case, the asymptotic limit is given by  $-\beta$  when  $\beta > 29/25 = 1.16$ . In Figure 2b, the upper two solid curves go to a power-law index of  $-\beta$  as  $F \rightarrow 0$ , and the lower two solid curves approach the monoluminous curve.

### 4.3. Average Redshift

An important difference between a monoluminous distribution and a broad luminosity distribution is that in the former the redshift and the flux have a one-to-one correspondence, while in the latter there is a distribution of redshift values for each flux value. From equation (20), one sees that the integrand is independent of  $F$ , and that the dependence on flux of the integral arises from the dependence of  $z_{max}$  on flux in equation (18). The shape of the redshift distribution is therefore independent of flux, and only the upper limit on  $z$  changes with flux. When the integrand rises monotonically with  $z$  for all  $z$ , the median value of  $z$  is a strong function of  $z_{max}$ , but when the integrand falls sufficiently rapidly above some value of  $z$ , the median value of  $z$  goes to a constant as  $z_{max}$  goes to infinity. From the discussion of the asymptotic behavior of equation (8), we know that the first instance occurs when  $L(z_0) \approx L_0$ , in which case the dependence of the burst number distribution on  $F$  is determined by the second index in either equation (12) or equation (16). In this case, the asymptotic behavior of the flux distribution is independent of the luminosity distribution function. The second instance arises when  $z_0 \approx 1$  or  $z_0 \approx 1/q_0$ , in which case the asymptotic behavior of the flux distribution is determined by the luminosity distribution.

Figure 3 shows the  $z$  distribution function for  $\beta = 0.6, 1.0, 1.4,$  and  $1.8$ . In the cases where  $\beta$  is large, the distribution peaks below  $z = 1$  and falls rapidly as  $z$  increases, so

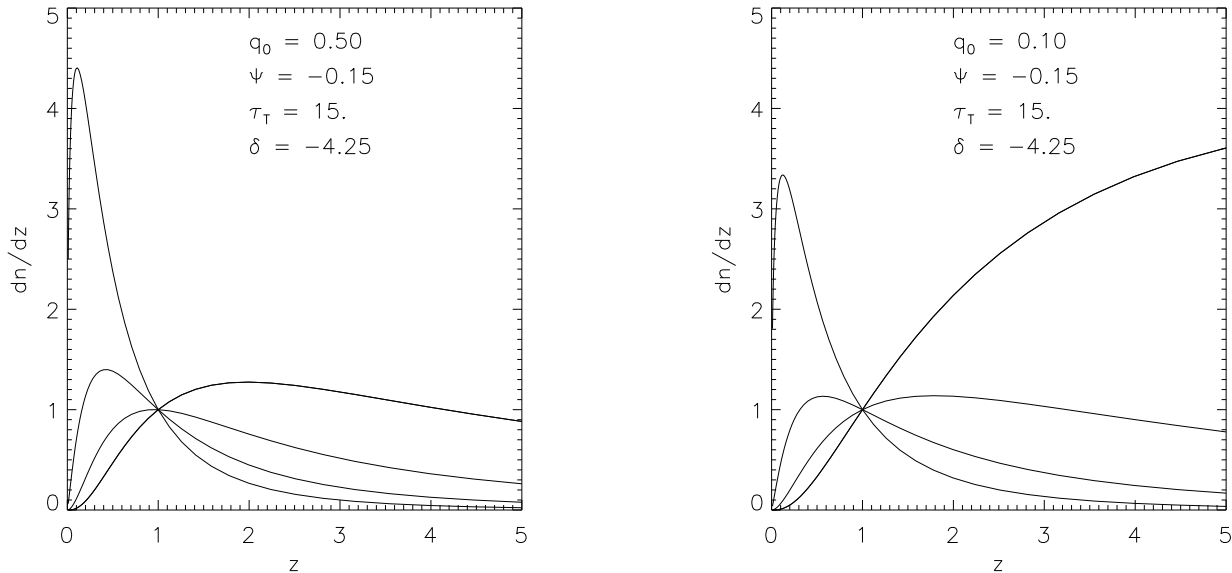


**Fig. 3**—Distribution of  $z$  for a power-law luminosity distribution. On each figure, the distribution curves for power-law indexes (from upper left to lower left) of  $\beta = 1.8, 1.4, 1.0,$  and  $0.6$  are plotted as functions of cosmological redshift  $z$ . The curves are normalized to unity at  $z = 1$ . The figures are for  $q_0 = 0.5$  (left) and  $0.1$  (right). The spectral parameters are  $\Psi = -0.15$  and  $\tau_T = 15$ .

the average value of  $z$  is a weak function of  $z_{max}$  when  $z_{max} \gg 1$ . As  $\beta$  decreases, the peak in the distribution function moves to higher  $z$ , until it disappears altogether, and the distribution function rises monotonically with  $z$ , so that the average value of  $z$  goes to  $z_{max}$ . Comparing Figure 3a to Figure 3b, one sees the behavior described in §3.1. When  $q_0 = 0.5$ , the integrand, and therefore the distribution in  $z$ , falls faster than  $z^{-1}$  as  $z \rightarrow \infty$  when  $\beta > 11/17$ . The three curves that satisfy this criterion exhibit the expected behavior. The curve that violates the inequality falls slowly as  $z$  rises. When  $q_0 = 0.1$ , the criterion is  $\beta > 29/25$ , which only two of the curves satisfy. Of the two curves violating the criterion, the  $\beta = 1$  curve falls slowly, while the  $\beta = 0.6$  curve continues to rise. When  $z > 10$ , which is not shown in the figure, both of these curves fall, since the  $\beta > 11/17$  inequality from equation (12) become the governing criterion.

Tests for the effects of the cosmological expansion rely on the average properties of gamma-ray bursts. Because the bursts of a given peak flux have a distribution of redshifts, a distinction must be made between the value of  $\langle z \rangle$  derived from time-dilation and the value derived from redshift. For the first, one is averaging  $1 + z$ , while for the second, one is averaging  $1/(1 + z)$ . The consequence is that the average value of  $z$  derived in the second

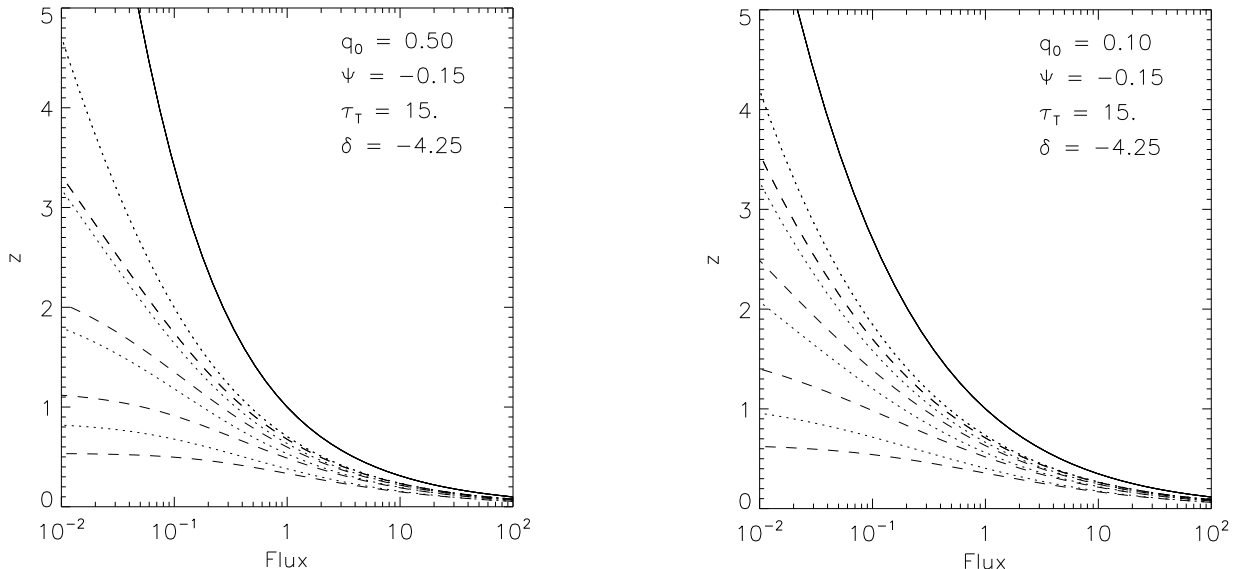


**Fig. 4**—Average values of  $z$  as a function of flux. The solid line gives the relationship between  $z$  and  $F$  from equation (18) with  $F_0 = 1$ . The dotted lines give  $\langle z \rangle$ , while the dashed lines give  $1/\langle(1+z)^{-1}\rangle - 1$ . The different lines are for, from bottom to top,  $\beta = 1.8, 1.4, 1.0$ , and  $0.6$ . The figures are for  $q_0 = 0.5$  (left) and  $0.1$  (right). The spectral parameters are  $\Psi = -0.15$  and  $\tau_T = 15$ .

case is smaller than in the first. This is shown in Figure 4, where  $\langle z \rangle$  is plotted as dotted lines, and  $1/\langle(1+z)^{-1}\rangle - 1$  is plotted as dashed lines for the values of  $\beta$  given in Figure 2. The curves go to a constant as  $z \rightarrow \infty$  when they satisfy the criterion on  $\beta$  that makes  $-\beta$  the asymptotic power-law index of the flux distribution.

## 5. Fitting the BATSE Flux Distribution

I use  $\chi^2$  minimization to fit the model flux distributions given in §4 to the flux distribution for a subset of gamma-ray bursts from the BATSE 3B catalog. This catalog gives the peak fluxes in the energy range of 50 keV to 300 keV for 869 gamma-ray bursts on three different time scales: 64 ms, 256 ms, and 1024 ms. The subset I use comprises the bursts that are not overwrites of a preceding burst, that have a T90 duration  $\geq 2$  s (where T90 is the time over which 90 % of the burst energy is emitted), and that have a peak flux on the 256 ms timescale of  $0.7 \text{ cm}^{-2} \text{ s}^{-1} < F < 110.9 \text{ cm}^{-2} \text{ s}^{-1}$ . There are 396 gamma-ray bursts that meet these criteria.

The upper threshold is for computational convenience, and it has no effect on the model fits. The lower threshold is to avoid the effects of the variable detector threshold and the detector geometry. The BATSE instrument triggers on a gamma-ray burst if the count rate exceeds a threshold count rate in at least two detectors. This count rate is set by integrating the background for 17 s intervals and calculating from this the standard deviation for counts on each of the three timescales given above. The trigger threshold is a multiple of this standard deviation; usually 5.5 standard deviations is chosen. Because the background fluctuates by a factor of 2 over the 90 minute orbit, the trigger threshold is variable. Because the trigger is in counts rather than in flux, because the detector geometry is an octahedron, and because Earth scatters burst radiation to the experiment, the flux threshold is angle dependent. These various effects cause an undercounting of gamma-ray bursts of low flux. The choice of  $0.7 \text{ cm}^{-2} \text{ s}^{-1}$  on the 256 ms timescale as a lower limit overcomes these difficulties (Pendleton et al. 1996).

For 90 minutes after a trigger, the threshold is raised so that if a particularly bright burst occurs, it is observed by the instrument. Such bursts, which are called overwrites, must be dropped from the sample, because they represent an overcounting of bright bursts relative to dim bursts.

The choice of timescales affects the choice of cosmological model. The reason is that if the burst pulse carrying the peak flux is fully resolved in time, then the cosmological redshift comes into the peak flux through the Lorentz boost of the flux, but if the pulse is much shorter than the instrument timescale, all photons in the pulse arrive inside that timescale regardless of time dilation. The time dilation of the emission therefore drops out of the problem, and the peak-flux has one more factor of  $(1 + z)$  than it does for the time-resolved pulse. I desire a timescale that resolves the time-behavior of most gamma-ray bursts without introducing large errors in the flux measurement from counting statistics. I compare in Figure 5 the peak fluxes of the 396 bursts in my sample. If two time scales each resolve the time-dependent variation of the flux, the peak flux measured on each should be equal within counting statistics. In Figure 5a, each burst is plotted on the 256 ms–1024 ms timescale plane, and in Figure 5b, each is plotted on the 64 ms–256 ms plane. The upper diagonal line represents equal fluxes on both timescales, which occurs when a pulse is fully time resolved. The lower diagonal line represents the short timescale having a peak flux that is 4 times the peak flux for the long timescale, which is what occurs when the pulse is much shorter than the short timescale. One sees that the clustering along the line of equality is stronger for Figure 5b than for Figure 5a, showing that the 256 ms timescale resolves most burst while the 1024 ms timescale leaves a large fraction of bursts unresolved. The percentage of bursts in Figure 5a that have a 256 ms peak flux that is more than a factor of 2 larger than the 1024 ms peak flux is 2.6%, while the percentage in Figure 5b that

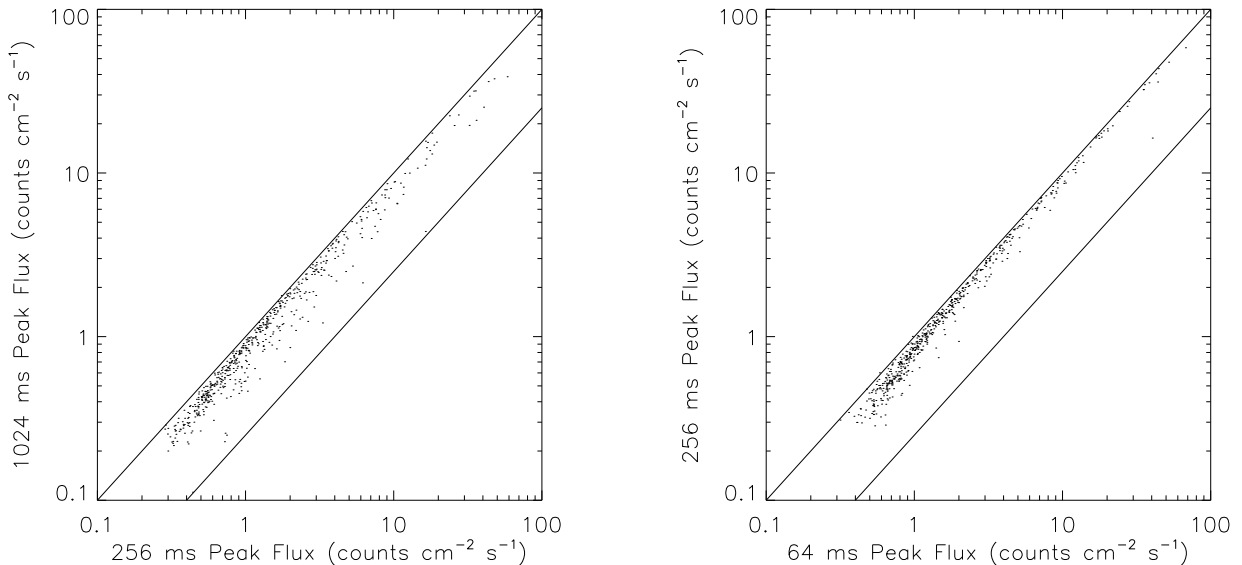


**Fig. 5**—Peak flux scatter plot. The gamma-ray bursts from the BATSE 3B catalog that have a duration measure  $T_{90} > 2$  s are plotted by their (left) 256 and 1024 ms peak fluxes and their (right) 64 and 256 ms peak fluxes in the 50 keV to 300 keV energy band. The upper diagonal line on each plot gives flux equality, while the lower diagonal on each gives a ratio of 1 to 4 in the two peak fluxes.

have a 64 ms peak flux that is more than a factor of 2 larger than the 256 ms peak flux is 0.7%. For a factor of  $\sqrt{2}$ , these percentages are 19.8% and 10.2% respectively. This is why the 256 ms timescale is used.

Some bursts have durations that are of order the sampling timescale. For these bursts, the time structure cannot be resolved, so a lower limit on the gamma-ray burst duration is warranted. The duration distribution is bimodal, with a local minimum at 2 s. This value is therefore a reasonable lower limit on  $T_{90}$  in the sample.

The burst distribution is summed into 22 bins that uniformly spanning  $\log F$  between  $0.7 \text{ cm}^{-2} \text{ s}^{-1}$  and  $110.9 \text{ cm}^{-2} \text{ s}^{-1}$ . Then, going from the highest flux bin to the lowest flux bin, each bin with fewer than 20 bursts is added to the bin immediately lower in flux. The purpose of this is to make gaussian statistics the correct description of the number of bursts in each bin. This lowers the number of bins to 11.

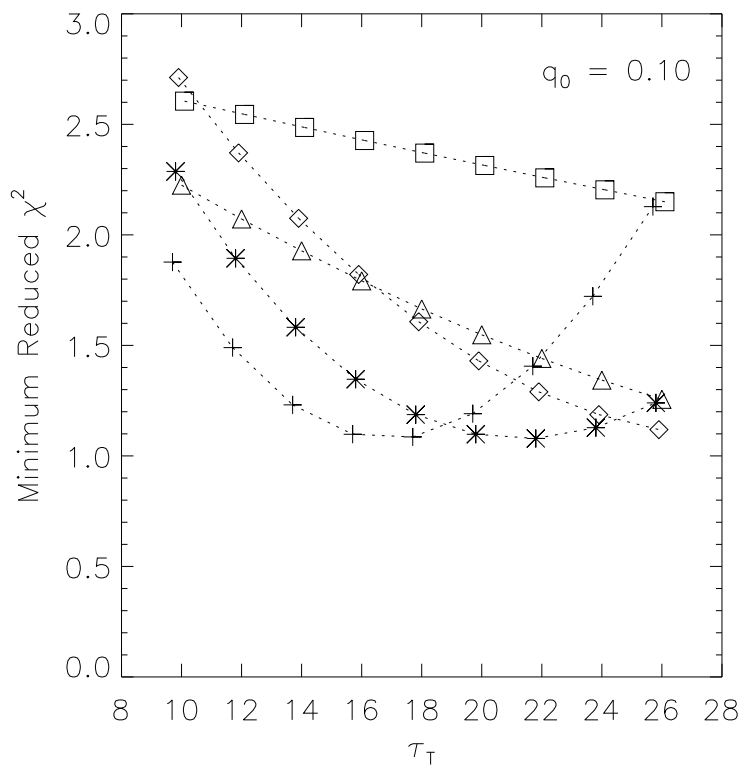
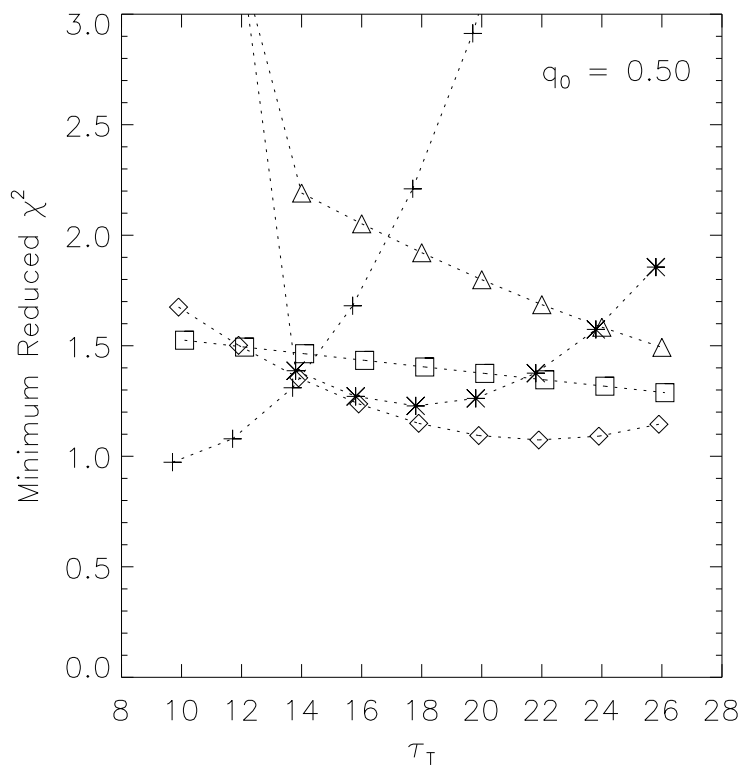


**Fig. 6**—Reduced  $\chi^2$  for fits of monoluminous peak-flux distributions to the BATSE data. The x-axis is the spectral parameter  $\tau_T$ , and the various sets of points are for  $\Psi = -0.10$  (+),  $-0.12$  (\*),  $-0.14$  ( $\diamond$ ),  $-0.16$  ( $\triangle$ ), and  $-0.18$  ( $\square$ ). In the upper figure,  $q_0 = 0.5$ , and in the lower figure,  $q_0 = 0.1$ .



TABLE 1  
MONOLUMINOSITY,  $q_0 = 0.5$

$\Psi^a$	$\tau_T^a$	Reduced $\chi^2{}^b$	$F_0^c$	$\sigma_{F_0}^d$	$\frac{1+z_1}{1+z_{10}}^e$
-0.10	10	1.0	1.3	0.3	1.76
-0.10	12	1.1	1.3	0.3	1.80
-0.10	14	1.3	1.3	0.3	1.85
-0.10	16	1.7	1.4	0.3	1.90
-0.10	18	2.2	1.4	0.3	1.95
-0.10	20	2.9	1.4	0.3	2.01
-0.10	22	3.8	1.4	0.3	2.08
-0.10	24	4.9	1.4	0.3	2.15
-0.12	10	6.8	3.4	0.9	2.08
-0.12	12	3.4	1.8	0.5	1.88
-0.12	14	1.4	2.1	0.4	1.99
-0.12	16	1.3	2.2	0.4	2.05
-0.12	18	1.2	2.2	0.4	2.11
-0.12	20	1.3	2.2	0.4	2.18
-0.12	22	1.4	2.2	0.4	2.26
-0.12	24	1.6	2.2	0.3	2.35
-0.14	10	1.7	1.7	0.4	1.77
-0.14	12	1.5	1.7	0.4	1.79
-0.14	14	1.4	1.7	0.4	1.82
-0.14	16	1.2	1.7	0.4	1.85
-0.14	18	1.1	1.8	0.4	1.88
-0.14	20	1.1	1.8	0.4	1.91
-0.14	22	1.1	1.8	0.4	1.94
-0.14	24	1.1	1.8	0.4	1.97
-0.16	10	5.4	2.3	0.7	1.81
-0.16	12	3.2	1.7	0.5	1.75
-0.16	14	2.2	1.9	0.4	1.78
-0.16	16	2.1	1.9	0.4	1.80
-0.16	18	1.9	1.9	0.4	1.81
-0.16	20	1.8	1.9	0.4	1.83
-0.16	22	1.7	1.9	0.4	1.84
-0.16	24	1.6	1.9	0.4	1.86
-0.18	10	1.5	1.1	0.3	1.61
-0.18	12	1.5	1.1	0.3	1.61
-0.18	14	1.5	1.1	0.3	1.61
-0.18	16	1.4	1.1	0.3	1.61
-0.18	18	1.4	1.1	0.3	1.61
-0.18	20	1.4	1.1	0.3	1.61
-0.18	22	1.3	1.1	0.3	1.62
-0.18	24	1.3	1.1	0.3	1.62

<sup>a</sup>Spectral parameters that are defined in §3 and held constant in the  $\chi^2$  minimization.

<sup>b</sup>For 9 degrees of freedom.

<sup>c</sup>The best fit value of the peak flux normalization in the 50keV to 300keV energy band in units of  $\text{photons cm}^{-2} \text{s}^{-1}$ .

<sup>d</sup>The formal standard deviation for  $F_0$  in units of  $\text{photons cm}^{-2} \text{s}^{-1}$ .

<sup>e</sup>The redshifts  $z_1$  and  $z_{10}$  at the values of  $z$  at the mean fluxes for the first and tenth data bins from the left in Fig. 7 of  $0.79 \text{ cm}^{-2} \text{ s}^{-1}$  and  $10.5 \text{ cm}^{-2} \text{ s}^{-1}$  respectively.

TABLE 2  
MONOLUMINOSITY,  $q_0 = 0.1$

$\Psi^a$	$\tau_T^a$	Reduced $\chi^2{}^b$	$F_0^c$	$\sigma_{F_0}^d$	$\frac{1+z_1}{1+z_{10}}^e$
-0.10	10	1.9	4.1	1.1	1.94
-0.10	12	1.5	4.0	1.0	2.00
-0.10	14	1.2	4.0	1.0	2.07
-0.10	16	1.1	3.9	0.9	2.15
-0.10	18	1.1	3.9	0.9	2.24
-0.10	20	1.2	3.8	0.8	2.34
-0.10	22	1.4	3.8	0.7	2.46
-0.10	24	1.7	3.8	0.7	2.60
-0.12	10	2.3	4.0	1.1	1.87
-0.12	12	1.9	3.9	1.1	1.91
-0.12	14	1.6	3.8	1.0	1.95
-0.12	16	1.3	3.8	1.0	1.99
-0.12	18	1.2	3.8	0.9	2.05
-0.12	20	1.1	3.7	0.9	2.10
-0.12	22	1.1	3.7	0.8	2.16
-0.12	24	1.1	3.7	0.8	2.23
-0.14	10	2.7	3.8	1.1	1.80
-0.14	12	2.4	3.7	1.1	1.83
-0.14	14	2.1	3.7	1.0	1.85
-0.14	16	1.8	3.6	1.0	1.87
-0.14	18	1.6	3.6	1.0	1.90
-0.14	20	1.4	3.5	0.9	1.93
-0.14	22	1.3	3.5	0.9	1.96
-0.14	24	1.2	3.5	0.9	1.99
-0.16	10	2.2	2.6	0.8	1.70
-0.16	12	2.1	2.6	0.8	1.71
-0.16	14	1.9	2.6	0.8	1.72
-0.16	16	1.8	2.6	0.8	1.73
-0.16	18	1.7	2.6	0.8	1.74
-0.16	20	1.5	2.6	0.8	1.76
-0.16	22	1.4	2.6	0.8	1.77
-0.16	24	1.3	2.6	0.8	1.78
-0.18	10	2.6	2.4	0.8	1.65
-0.18	12	2.5	2.4	0.8	1.66
-0.18	14	2.5	2.4	0.8	1.66
-0.18	16	2.4	2.4	0.8	1.66
-0.18	18	2.4	2.4	0.8	1.66
-0.18	20	2.3	2.4	0.8	1.67
-0.18	22	2.3	2.4	0.8	1.67
-0.18	24	2.2	2.4	0.8	1.67

<sup>a</sup>Spectral parameters that are defined in §3 and held constant in the  $\chi^2$  minimization.

<sup>b</sup>For 9 degrees of freedom.

<sup>c</sup>The best fit value of the peak flux normalization in the 50keV to 300keV energy band in units of  $\text{photons cm}^{-2} \text{s}^{-1}$ .

<sup>d</sup>The formal standard deviation for  $F_0$  in units of  $\text{photons cm}^{-2} \text{s}^{-1}$ .

<sup>e</sup>The redshifts  $z_1$  and  $z_{10}$  at the values of  $z$  at the mean fluxes for the first and tenth data bins from the left in Fig. 7 of  $0.79 \text{ cm}^{-2} \text{ s}^{-1}$  and  $10.5 \text{ cm}^{-2} \text{ s}^{-1}$  respectively.

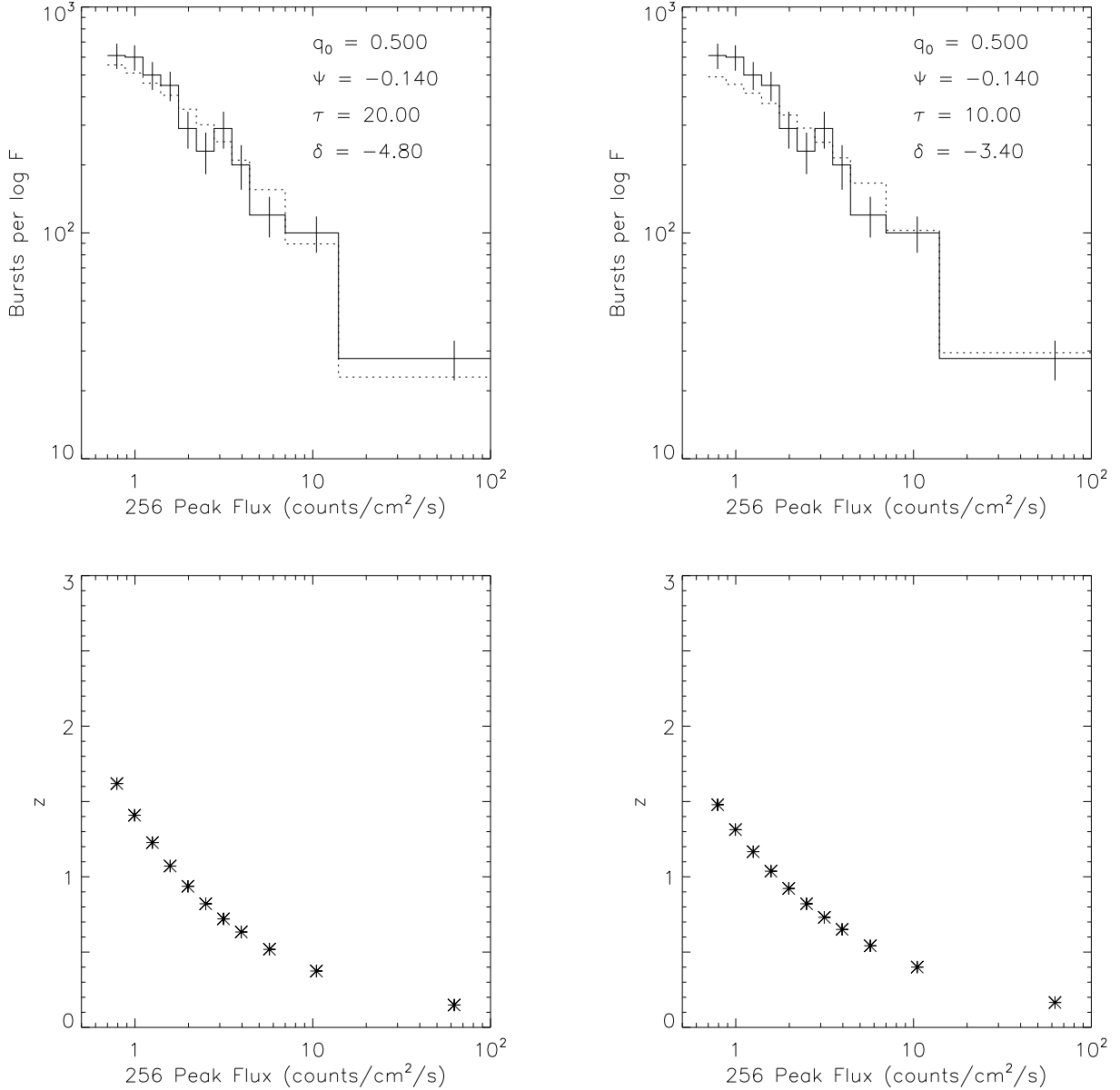


**Fig. 7**—Examples of monoluminous peak-flux distributions fit to BATSE data. In the upper figures, the solid curve gives the BATSE data with statistical errors and the dotted curve gives the expected value from the best fit model. The peak flux is for the 256 ms timescale in the 50 keV to 300 keV energy band. The lower figures give the value of  $z$  as a function of peak flux for the best fit model. For both models,  $\Psi = -0.14$  and  $q_0 = 0.5$ . On the left, the reduced  $\chi^2$  is 1.1 for 9 degrees of freedom with  $\tau_T = 20$ , and, on the right, the reduced  $\chi^2$  is 1.7 with  $\tau_T = 10$ .

### 5.1. Monoluminosity Distribution

In fits of the monoluminous flux distribution to the BATSE data, I fix the values of  $q_0$ ,  $\Psi$ , and  $\tau_T$ . These variables are set by data that is independent of the peak flux distribution. In particular, the values of  $\Psi$  and  $\tau_T$  are set by fitting gamma-ray burst spectra. Generally one finds  $-0.16 < \Psi < -0.12$  and  $10 < \tau_T < 30$  from fits to the spectra of bursts observed by BATSE (Brainerd et al. 1996b). This leaves two free parameters in the  $\chi^2$  minimization,  $F_0$  and  $N_0$ , giving 9 degrees of freedom in the minimization. The results are given in Tables 1 and 2 for  $\Psi$  ranging from  $-0.10$  to  $-0.18$  and  $\tau_T$  ranging from 10 to 26. In these tables, the first and second columns give the values at which  $\Psi$  and  $\tau_T$  are held, the third column gives the value of reduced  $\chi^2$  from the minimization, the fourth column gives the value of  $F_0$  derived from the minimization, and the fifth column gives the formal error on  $F_0$ . The final column gives the ratio of  $1 + z_1$  to  $1 + z_{10}$ , where, counting from the lowest to the highest peak-flux rate,  $z_1$  is the redshift at the center of the first data bin and  $z_{10}$  is the redshift at the center of the tenth data bin. These bins are centered on the peak-flux rates of  $0.79 \text{ cm}^{-2} \text{ s}^{-1}$  and  $10.5 \text{ cm}^{-2} \text{ s}^{-1}$  respectively. The minimum values of reduced  $\chi^2$  given in the tables are plotted against  $\tau_T$  in Figure 6.

The minimum value of  $\chi^2$  is strongly dependent on the values chosen for  $\Psi$  and  $\tau_T$ , and only for specific combinations of these values are good fits found. The best value of reduced  $\chi^2$  is  $\approx 1.0$ , which has an expectation of 0.5 for 9 degrees of freedom; an expectation of  $\approx 0.01$  is found for a reduced  $\chi^2$  of 2.4. For a given value of  $q_0$ , the value of  $\tau_T$  that gives a good fit increases rapidly as  $\Psi$  decrease, that is, as the value of  $E_p$  decreases. The characteristic values of  $\tau_T$  and  $\Psi$  one derives from fits to the spectra ( $\tau_T \approx 20$  and  $\Psi \approx -0.14$ ) produce a model fit to the flux distribution with a reduced  $\chi^2$  of 1.1 when  $q_0 = 0.5$ , and a reduced  $\chi^2$  of 1.9 when  $q_0 = 0.1$ . The values of  $F_0$  that one derives vary little as  $\Psi$  and  $\tau_T$  vary; it is  $1\text{--}2 \text{ cm}^{-2} \text{ s}^{-1}$  for  $q_0 = 0.5$ , and it is  $2.5\text{--}4 \text{ cm}^{-2} \text{ s}^{-1}$  for  $q_0 = 0.1$ . As a consequence, the value of  $z$  at the BATSE threshold is  $\approx 1.5\text{--}2.5$ .

Figure 7 shows two specific examples of model fits, one of which fits the data well, the other poorly. When the model fits the data poorly, it is because the model breaks more rapidly away from a  $-5/2$  power law than does the data. These figures also show the variation of  $z$  with  $F$ .

### 5.2. Cutoff Power-Law Luminosity Distribution

The flux distribution for the power-law luminosity distribution has three free parameters:  $F_0$ ,  $N_0$ , and  $\beta$ . Because  $q_0$ ,  $\Psi$ , and  $\tau_T$  are fixed parameters, the model fits have

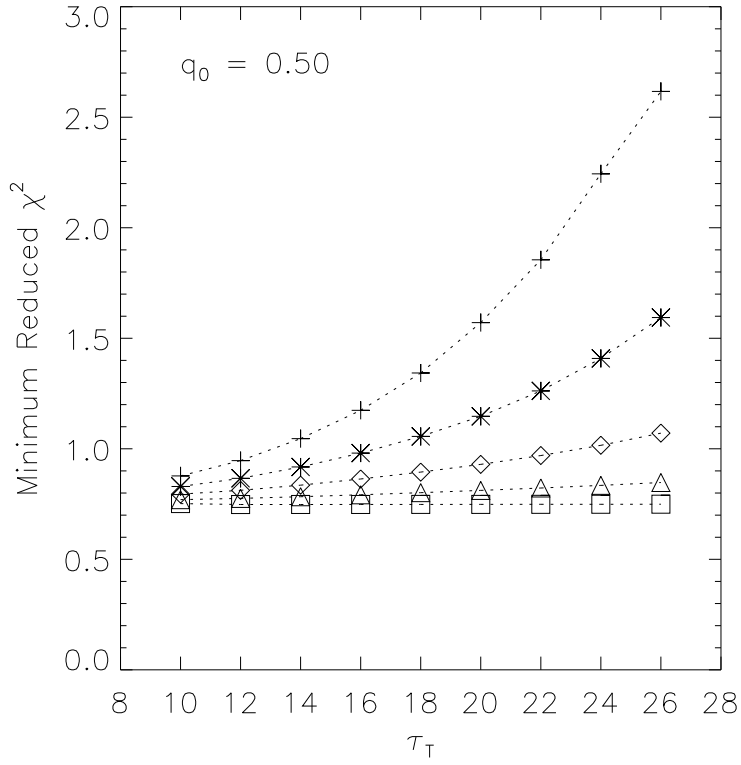


**Fig. 8**—Reduced  $\chi^2$  for fits of power-law luminosity peak-flux distributions to BATSE data. As in Fig. 6.

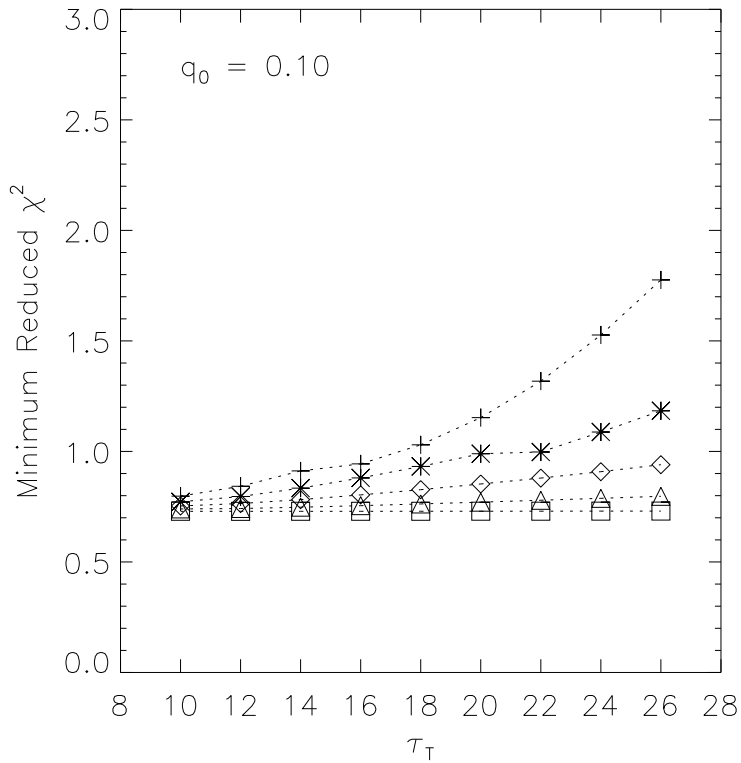


TABLE 3  
POWER LAW LUMINOSITY,  $q_0 = 0.5$

$\Psi^a$	$\tau_T^a$	Reduced $\chi^2{}^b$	$F_0^c$	$\sigma_{F_0}^d$	$\beta^e$	$\sigma_\beta^f$	Dilation Ratio <sup>g</sup>	Redshift Ratio <sup>h</sup>
-0.10	10	0.9	6.3	9.9	1.41	0.70	1.55	1.38
-0.10	12	0.9	6.3	9.6	1.40	0.77	1.62	1.43
-0.10	14	1.0	6.5	9.1	1.37	0.83	1.71	1.48
-0.10	16	1.2	6.6	8.2	1.32	0.86	1.82	1.55
-0.10	18	1.3	6.8	6.9	1.27	0.84	1.96	1.63
-0.10	20	1.6	6.9	5.5	1.22	0.77	2.11	1.72
-0.10	22	1.9	7.2	4.4	1.19	0.64	2.28	1.80
-0.10	24	2.2	7.2	3.4	1.16	0.54	2.44	1.88
-0.12	10	0.8	5.9	10.0	1.46	0.63	1.47	1.33
-0.12	12	0.9	5.9	10.0	1.45	0.68	1.51	1.35
-0.12	14	0.9	6.0	9.8	1.43	0.74	1.56	1.39
-0.12	16	1.0	6.2	9.5	1.41	0.79	1.62	1.43
-0.12	18	1.1	6.3	8.9	1.37	0.83	1.69	1.47
-0.12	20	1.1	6.5	8.1	1.34	0.84	1.77	1.53
-0.12	22	1.3	6.6	7.1	1.30	0.82	1.87	1.58
-0.12	24	1.4	6.8	6.1	1.26	0.78	1.97	1.64
-0.14	10	0.8	5.5	10.1	1.50	0.57	1.40	1.28
-0.14	12	0.8	5.6	10.1	1.49	0.60	1.42	1.30
-0.14	14	0.8	5.6	10.2	1.49	0.64	1.45	1.31
-0.14	16	0.9	5.7	10.1	1.47	0.68	1.48	1.33
-0.14	18	0.9	5.8	10.0	1.46	0.72	1.51	1.36
-0.14	20	0.9	5.9	9.8	1.44	0.75	1.55	1.38
-0.14	22	1.0	6.0	9.5	1.41	0.78	1.60	1.41
-0.14	24	1.0	6.2	9.0	1.39	0.80	1.64	1.45
-0.16	10	0.8	5.2	10.1	1.53	0.51	1.35	1.24
-0.16	12	0.8	5.2	10.2	1.53	0.53	1.36	1.25
-0.16	14	0.8	5.3	10.3	1.53	0.55	1.37	1.26
-0.16	16	0.8	5.3	10.4	1.52	0.57	1.38	1.27
-0.16	18	0.8	5.4	10.5	1.52	0.60	1.39	1.28
-0.16	20	0.8	5.4	10.5	1.51	0.62	1.41	1.29
-0.16	22	0.8	5.5	10.6	1.50	0.65	1.43	1.30
-0.16	24	0.8	5.5	10.6	1.49	0.67	1.45	1.31
-0.18	10	0.8	5.2	11.0	1.58	0.44	1.29	1.20
-0.18	12	0.7	5.2	11.0	1.58	0.45	1.29	1.20
-0.18	14	0.7	5.3	11.2	1.58	0.45	1.30	1.21
-0.18	16	0.7	5.3	11.3	1.58	0.46	1.30	1.21
-0.18	18	0.7	5.3	11.5	1.58	0.47	1.30	1.21
-0.18	20	0.7	5.3	11.6	1.58	0.48	1.31	1.21
-0.18	22	0.7	5.3	11.8	1.58	0.49	1.31	1.21
-0.18	24	0.7	5.3	11.9	1.57	0.50	1.31	1.22

<sup>a</sup>Spectral parameters that are defined in §3 and held constant in the  $\chi^2$  minimization.

<sup>b</sup>For 8 degrees of freedom.

<sup>c</sup>The best fit value of the peak flux normalization in the 50keV to 300keV energy band in units of photons  $\text{cm}^{-2} \text{s}^{-1}$ .

<sup>d</sup>The formal standard deviation for  $F_0$  in units of photons  $\text{cm}^{-2} \text{s}^{-1}$ .

<sup>e</sup>The best fit value of the luminosity function power law index.

<sup>f</sup>The formal standard deviation for  $\beta$ .

<sup>g</sup>The ratio of the average time dilation for the mean fluxes of the first and tenth bins of Fig. 9 of 0.79  $\text{cm}^{-2} \text{s}^{-1}$  and 10.5  $\text{cm}^{-2} \text{s}^{-1}$  respectively.

<sup>h</sup>The ratio of average spectral redshift for the mean fluxes used for the Dilation Ratio.

TABLE 4  
POWER LAW LUMINOSITY,  $q_0 = 0.1$

$\Psi^a$	$\tau_T^a$	Reduced $\chi^2{}^b$	$F_0^c$	$\sigma_{F_0}^d$	$\beta^e$	$\sigma_\beta^f$	Dilation Ratio <sup>g</sup>	Redshift Ratio <sup>h</sup>
-0.10	10	0.8	7.1	15.2	1.31	1.08	1.57	1.44
-0.10	12	0.8	7.2	15.1	1.29	1.21	1.62	1.49
-0.10	14	0.9	7.3	14.9	1.24	1.38	1.70	1.55
-0.10	16	0.9	8.1	14.4	1.08	1.69	1.85	1.68
-0.10	18	1.0	8.6	13.5	0.96	1.90	1.98	1.80
-0.10	20	1.2	8.9	12.1	0.85	2.00	2.13	1.92
-0.10	22	1.3	9.3	10.6	0.77	1.96	2.28	2.05
-0.10	24	1.5	9.7	9.1	0.72	1.78	2.44	2.16
-0.12	10	0.8	6.7	14.9	1.38	0.91	1.48	1.37
-0.12	12	0.8	6.7	15.0	1.37	1.00	1.52	1.40
-0.12	14	0.8	6.8	15.1	1.35	1.10	1.56	1.43
-0.12	16	0.9	7.0	15.0	1.31	1.22	1.62	1.48
-0.12	18	0.9	7.1	14.7	1.27	1.35	1.68	1.53
-0.12	20	1.0	7.4	14.2	1.21	1.49	1.75	1.59
-0.12	22	1.0	8.1	13.3	1.04	1.71	1.89	1.72
-0.12	24	1.1	8.3	12.2	0.98	1.76	1.97	1.78
-0.14	10	0.8	6.2	14.7	1.44	0.78	1.42	1.32
-0.14	12	0.8	6.3	14.9	1.44	0.83	1.44	1.33
-0.14	14	0.8	6.3	15.0	1.43	0.89	1.46	1.35
-0.14	16	0.8	6.4	15.1	1.41	0.95	1.49	1.37
-0.14	18	0.8	6.5	15.2	1.39	1.03	1.52	1.40
-0.14	20	0.9	6.7	15.2	1.36	1.11	1.56	1.43
-0.14	22	0.9	6.8	15.0	1.33	1.20	1.59	1.46
-0.14	24	0.9	7.0	14.7	1.29	1.28	1.64	1.50
-0.16	10	0.7	6.1	15.4	1.51	0.65	1.36	1.27
-0.16	12	0.7	6.2	15.5	1.51	0.67	1.37	1.27
-0.16	14	0.7	6.2	15.7	1.50	0.70	1.38	1.28
-0.16	16	0.8	6.2	15.9	1.50	0.73	1.39	1.29
-0.16	18	0.8	6.3	16.0	1.49	0.76	1.40	1.30
-0.16	20	0.8	6.3	16.2	1.48	0.80	1.42	1.31
-0.16	22	0.8	6.4	16.3	1.47	0.83	1.43	1.32
-0.16	24	0.8	6.5	16.4	1.46	0.88	1.45	1.34
-0.18	10	0.7	5.7	15.0	1.54	0.58	1.31	1.23
-0.18	12	0.7	5.7	15.2	1.54	0.59	1.32	1.23
-0.18	14	0.7	5.7	15.4	1.54	0.60	1.32	1.24
-0.18	16	0.7	5.7	15.6	1.54	0.61	1.32	1.24
-0.18	18	0.7	5.7	15.8	1.54	0.62	1.32	1.24
-0.18	20	0.7	5.7	16.1	1.54	0.64	1.33	1.24
-0.18	22	0.7	5.7	16.3	1.54	0.65	1.33	1.24
-0.18	24	0.7	5.8	16.5	1.53	0.67	1.33	1.25

<sup>a</sup>Spectral parameters that are defined in §3 and held constant in the  $\chi^2$  minimization.

<sup>b</sup>For 8 degrees of freedom.

<sup>c</sup>The best fit value of the peak flux normalization in the 50keV to 300keV energy band in units of photons  $\text{cm}^{-2} \text{s}^{-1}$ .

<sup>d</sup>The formal standard deviation for  $F_0$  in units of photons  $\text{cm}^{-2} \text{s}^{-1}$ .

<sup>e</sup>The best fit value of the luminosity function power law index.

<sup>f</sup>The formal standard deviation for  $\beta$ .

<sup>g</sup>The ratio of the average time dilation for the mean fluxes of the first and tenth bins of Fig. 9 of 0.79  $\text{cm}^{-2} \text{s}^{-1}$  and 10.5  $\text{cm}^{-2} \text{s}^{-1}$  respectively.

<sup>h</sup>The ratio of average spectral redshift for the mean fluxes used for the Dilation Ratio.

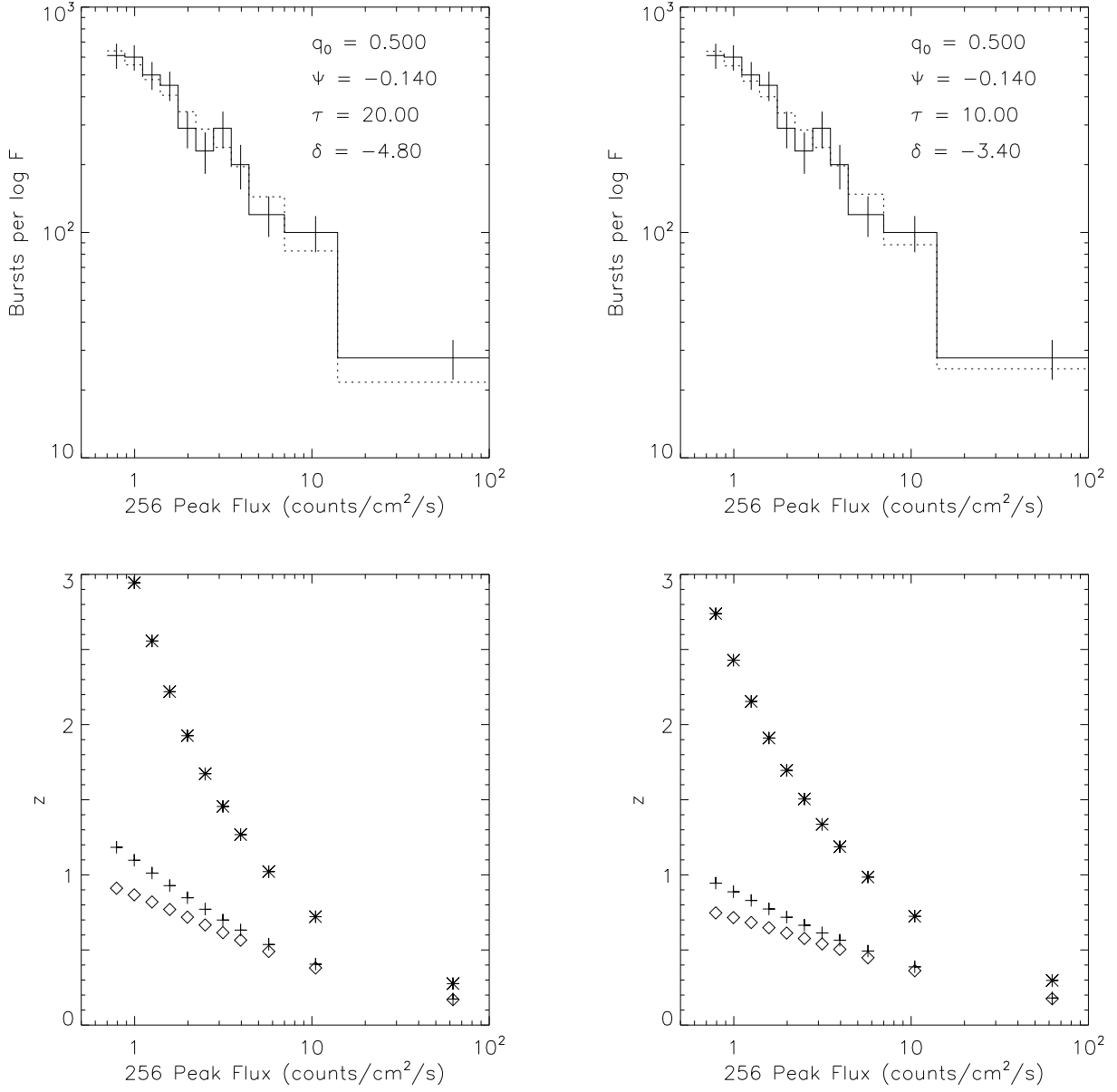


**Fig. 9**—Examples of power-law luminosity peak-flux distributions fit to BATSE data. Upper figures are as in Fig. 7. In the lower figures, the value of  $z_{max}$  is given by  $\star$ , the value of  $\langle z \rangle$  is given by  $+$ , and the value of  $1/\langle(1+z)^{-1}\rangle - 1$  is given by  $\diamond$ . On the left, the reduced  $\chi^2$  is 0.9 for 8 degrees of freedom with  $\tau_T = 20$ , and on the right, it is 0.8 with  $\tau_T = 10$ . The value of  $z_{min}$  for the lowest bin in the lower left figure is 3.39, which is off the plot.



8 degrees of freedom. The introduction of a power-law luminosity distribution improves the ability of a cosmological gamma-ray burst model to fit the observed flux distribution, with most values of  $\Psi$ ,  $\tau_T$ , and  $q_0$  producing acceptable values of reduced  $\chi^2$ . These values are plotted in Figure 8, and the results of the model fits are listed in Tables 3 and 4. The first five columns in these tables are as in Tables 1 and 2. The sixth column is the derived value of  $\beta$ , the seventh column is the formal error for  $\beta$ , the eighth column is the ratio of the average time dilation factor for the first data bin to the average time dilation factor for the tenth data bin, and the tenth column is the ratio of the average redshift factor for the first data bin to the average redshift factor for the tenth data bin. Two of the model fits listed in Table 3 are plotted in Figure 9. For the values of  $\Psi$  and  $\tau_T$  consistent with observed gamma-ray burst spectra, fits to the flux distribution produce values of reduced  $\chi^2 \approx 0.8$ .

The derived values of  $F_0$  range between  $5 \text{ cm}^{-2} \text{ s}^{-1}$  and  $10 \text{ cm}^{-2} \text{ s}^{-1}$ , with the best values of  $\chi^2$  having the lowest values of  $F_0$ . But the formal errors for  $F_0$  are of order  $10 \text{ cm}^{-2} \text{ s}^{-1}$ . Such values for  $F_0$  imply isotropic burst luminosities of  $\approx 2 \times 10^{51} \text{ ergs s}^{-1}$  when  $H_0 = 75 \text{ km s}^{-1} \text{ Mpc}^{-1}$  in the 50 keV to 300 keV energy band. The value of  $\beta$  ranges between 0.7 and 1.6, with the highest values occurring for the lowest values of  $\chi^2$ , but again the error is large, of order 0.5. These values of  $\beta$  are somewhat smaller than the value of  $\approx 1.9$  one would get from a pure power-law fit to the data. The data therefore do not go to sufficiently low flux to exhibit the asymptotic limit. The values of  $\beta$  found in this study imply that the number of bursts per decade luminosity changes slowly with luminosity. For instance, with  $\beta = 1.6$ , only 75% of the bursts are within a factor of 10 of the lower threshold. This shows that gamma-ray bursts do not need a steeply falling or a narrow luminosity distribution to reproduce the observations.

The large values of  $\beta$  in these fits imply that the redshift distribution function is strongly peaked at  $z < 1$ . The effect of this is clear in the lower halves of Figures 9a and 9b. The value of  $z_{max}$  for the bursts at threshold is generally  $\gtrsim 3$ . On the other hand, the average time dilation and redshift factors are relatively small and slowly varying. In Figure 9, the implied redshifts from averages over  $(1+z)$  and  $1/(1+z)$  are plotted. Even though  $z_{max} \gtrsim 3$ , the average redshifts are  $\lesssim 1$ . Comparing these figures to Figure 7 shows that the variation of the average  $z$  with  $F$  for the power-law luminosity model is less than the variation of  $z$  for the monoluminous model. For instance, in Figure 7a, the lowest flux bin, which is centered at  $0.79 \text{ cm}^{-2} \text{ s}^{-1}$ , has  $z = 1.62$  and the tenth bin, which is centered at  $10.5 \text{ cm}^{-2} \text{ s}^{-1}$ , has  $z = 0.37$ ; in contrast, in Figure 9a, the average values of  $z$  from the time dilation are 1.18 and 0.41 for these flux bins, and the average values of  $z$  from the spectral redshift are 0.91 and 0.38.

The values of  $z$  derived from fits to the peak flux distribution are lower but consistent

with the values of  $z$  derived from fits of the Compton attenuation spectral model to the spectra of bursts observed by BATSE. Spectral fits to relatively bright bursts (peak fluxes  $> 10 \text{ cm}^{-2} \text{ s}^{-1}$ ) produce  $0.5 < z < 4$  (Brainerd et al. 1996b). Given the large uncertainty in  $F_0$ , those results do not contradict the results presented above.

Three conclusions are evident. First, fits of the data to the monoluminous model are more sensitive to the spectral parameters than are fits to the power-law luminosity models. Second, the maximum redshifts that are consistent with the data are much larger when a luminosity function is present than when bursts are monoluminous. Third, the spectral redshift and time dilation from the cosmological expansion are weakened by the presence of a luminosity distribution.

## 6. Redshift and Time Dilation Tests

Researchers have sought evidence of a cosmological time dilation and spectral redshift in sets of gamma-ray bursts by comparing the characteristics of bursts at one flux to those at another. Such studies derive the ratio of the average time dilation (or redshift) at these two fluxes rather than the average value of  $z$  (Mitrofanov et al. 1994, 1996; Fenimore & Bloom 1995). When the bursts are monoluminous, this ratio goes to a constant as  $F \rightarrow \infty$ . From equation (7), with the spectrum set to a power law  $\propto \nu^\delta$ , the limiting value of the redshift ratio  $(1 + z_{dim}) / (1 + z_{bright})$  for the fluxes  $F_{dim} < F_{bright}$  is  $(F_{bright}/F_{dim})^{1/(2-\delta)}$  when  $1 \ll z \ll 1/q_0$  and  $(F_{bright}/F_{dim})^{-1/\delta}$  when  $z \gg 1/q_0$ . For a flux ratio of  $F_{bright}/F_{dim} = 10$  and a characteristic power-law index of  $\delta = -3$ , the first relationship gives 2.15 and the second gives 1.58. The upper plot of Figure 10a gives the behavior of  $(1 + z_{dim}) / (1 + z_{bright})$  as a function of  $F_{dim}$  for  $F_{bright}/F_{dim} = 10$ . The asymptotic behavior for small flux is evident in this figure. More striking is the maximum in each curve at  $F \approx 3 \times 10^{-2} F_0$ . The maximum is generally  $\lesssim 4$ , with the value of the peak decreasing with  $\Psi$  and  $q_0$ . The values of this ratio for the model fits discussed above are given in Tables 1 and 2 for  $F_{dim} = F_1 = 0.79 \text{ cm}^{-2} \text{ s}^{-1}$ , the flux at the center of the first flux bin, and  $F_{bright} = F_{10} = 10.5 \text{ cm}^{-2} \text{ s}^{-1}$ , the flux at the center of the tenth flux bin. The value of  $z$  at the center of bin 1 is  $z_1$ , and its value at the center of bin 10 is  $z_{10}$ . Note that this ratio is  $\lesssim 2$  in the tables. Figure 10b gives the results for  $F_{bright}/F_{dim} = 5$ . Lowering the ratio of fluxes dramatically decreases the redshift ratio curves.

Introducing a power-law luminosity function lowers the value of the average time dilation and redshift ratios from those found in the monoluminous model. In the lower plot of Figure 10a, one sees that the ratios of average time dilation are much smaller than in the monoluminosity case and that the peak value of the ratio is generally  $\lesssim 1.7$ . The

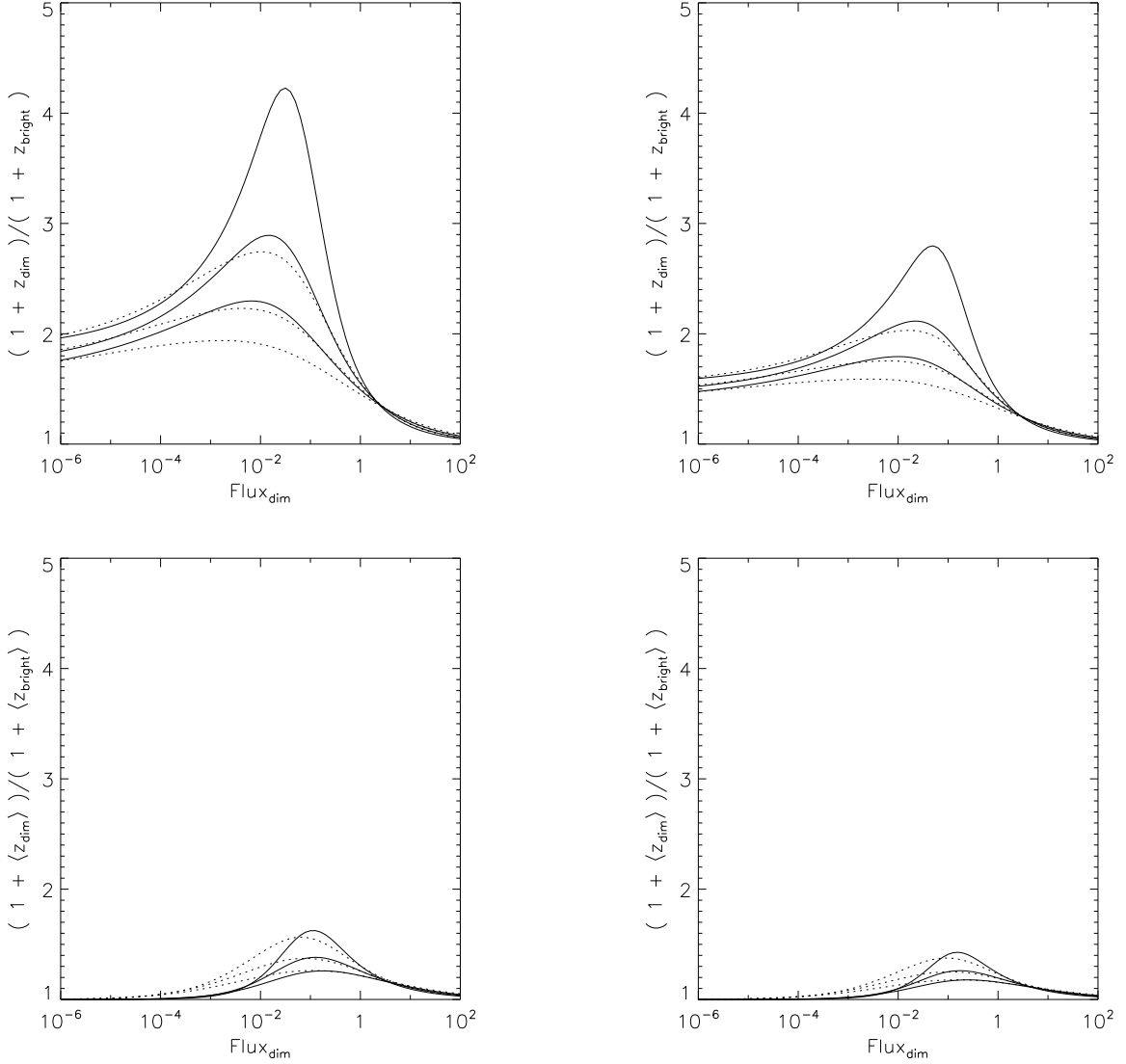


**Fig. 10**— $(1 + z_{dim}) / (1 + z_{bright})$  versus peak flux. The ratios of time dilation factors for various cosmological models are plotted. The cosmological redshifts  $z_{dim}$  and  $z_{bright}$  are the redshifts associated with  $F_{dim}$  and  $F_{bright}$ , where, on the left,  $F_{bright} = 10 F_{dim}$  and, on the right,  $F_{bright} = 5 F_{dim}$ . The upper figures are for the monoluminous model, with the solid lines for  $q_0 = 0.5$  and the dotted lines for  $q_0 = 0.1$ . The lower figures are for the power-law luminosity model with  $\beta = 1.6$  and the remaining parameters as in the upper figures. For these figures,  $z_{dim}$  and  $z_{bright}$  are average values of redshift. For all curves  $\tau_T = 18$ , and, from top to bottom in each figure, the curves have  $\Psi = -0.1, -0.14,$  and  $-0.18$ . The flux is normalized so that  $F_0 = 1$ , and it is measured in the 50 keV to 300 keV energy band.

time dilation and redshift ratios for the first and tenth bins for the model fits to the data are given in Tables 3 and 4. The time dilation and redshift ratios for values of reduced  $\chi^2$  near 0.8 are  $\lesssim 1.6$ . These values can be as low as  $\approx 1.20$  for some spectral parameters that produced good model fits to the flux distribution. This demonstrates that the cosmological effects are never large when a luminosity distribution determines the shape of the flux distribution, and that often the cosmological effects are slight, even though many bursts in the model have  $z \gtrsim 1$ . Again, going to a flux ratio of  $F_{bright}/F_{dim} = 5$  dramatically lowers these ratio curves.

Many studies report a correlation of the gamma-ray burst timescale with the peak flux, finding that the dim bursts are on average longer than the bright bursts. Examples of the tests producing positive results are wavelet analysis, the total normalized counts test (Norris et al. 1994), and the fitted pulse width test (Davis et al. 1994). One test, the peak aligned test (Mitrofanov et al. 1993) produces conflicting results, with some researchers finding a correlation in the BATSE data (Norris et al. 1994), and others finding no correlation in either the BATSE data (Mitrofanov et al. 1996) or the data from the APEX experiment on Phobos-2 (Mitrofanov et al. 1993). This is somewhat disheartening, because clear evidence of a correlation would give the discussion that follows more resonance, but there is no consensus on the issue, so I'll address both sides of it.

Those timescale studies that report a correlation generally find a dramatic effect. Norris et al. (1994) find that BATSE gamma-ray bursts with peak count rates above  $18000 \text{ s}^{-1}$  are  $\approx 2.25$  times as long as bursts with peak count rates between  $1400 \text{ s}^{-1}$  and  $2400 \text{ s}^{-1}$ . The actual time dilation ratio required to produce such an effect is much larger, because gamma-ray burst durations are photon-energy dependent. If the duration is proportional to  $\nu^{-0.23}$  (Mitrofanov et al. 1996), then a time dilation ratio of 2.8 is required. From Figure 10, one sees that a ratio of this size is impossible to achieve in the power-law luminosity model, and it is possible in the monoluminous model for only part of the available parameter space. As Fenimore & Bloom (1995) note, the monoluminous models produce a time dilation ratio of the required size at  $z_{dim} \gtrsim 6$ , which is inconsistent with the flux distribution. When the time dilation ratios for a factor of 10 difference in flux are calculated for the models in Tables 1–4, one finds that the monoluminous model produces ratios between 1.5 and 2 and the power-law luminosity model produces ratios between 1.2 and 1.5.

To be more precise about this, let us use the specific model of a  $q_0 = 0.1$  universe and a  $\Psi = -0.14$  and  $\tau_T = 20$  spectral model. For a power law luminosity, a fit to the peak flux distribution gives  $F_0 = 6.7 \text{ cm}^{-2} \text{ s}^{-1}$  and  $\beta = 1.36$ , while for a monoluminous distribution,  $F_0 = 3.5 \text{ cm}^{-2} \text{ s}^{-1}$ .

In Davis et al. (1994), time dilation ratios of  $1.9_{-0.44}^{+0.34}$ ,  $1.8_{-0.33}^{+0.38}$ , and  $1.6_{-0.47}^{+0.39}$  are found

from three different statistical tests when comparing bursts with count rates between 18000 and 250000 counts per second to those between 2400 and 4500 counts per second. These tests are all based on fitting with width of pulse structure within a burst, and are therefore dependent on the photon energy. Taking this lower count rate to be a photon flux of  $0.45 \text{ cm}^2 \text{ s}^{-1}$ , and taking the lower edge of the upper interval to be  $5.8 \text{ cm}^2 \text{ s}^{-1}$ , and assuming that the width of the pulses go as  $\nu^{-0.23}$ , one finds dilation ratios of 1.52 for the monoluminous model and 1.31 for the power-law luminosity model. Comparing the same upper count band to a lower range of 1400 to 2400 counts per second, the tests give ratios of  $2.0_{-0.47}^{+0.62}$ ,  $2.2_{-0.44}^{+0.72}$ , and  $1.8_{-0.51}^{+0.65}$ , while the monoluminous model gives 1.52, and the power-law luminosity model gives 1.41. These various tests produces results that are all larger than the monoluminous model by about one standard deviation, and larger than the power-law luminosity model by about one and one-half standard deviations. For the quoted errors, the monoluminous model produces a value that is one and one-half standard deviations above unity, and the power-law luminosity model produces a value that is less than one standard deviation from unity.

A test that compares the time between peaks, which is not energy dependent to the extent that the width of a single peak is, finds dilation ratios of 2.18 and 2.20 on the 256 ms timescale for two different selection criterion, with significances compared to unity of 0.013 and 0.0016 respectively (Norris et al. 1996). Assuming gaussian statistics, these significances correspond to 2.5 and 3.2 standard deviations from unity, so the standard deviations for these measures are 0.47 and 0.38 respectively. In the absence of energy dependence of the measured duration, the monoluminous model gives 1.73 and the power-law luminosity model gives 1.42. The observed result is of order a standard deviation above the monoluminous model and two standard deviations above the power-law luminosity model.

The one test that finds no evidence of a duration–peak flux correlation is the analysis of Mitrofanov et al. (1996). The peak-aligned method is used in this article to compare the average duration of bursts with different peak fluxes. It tests a different aspect of burst timescale than those just discussed, so the absence of a signal does not necessarily contradict these other tests. There is a contradiction with Norris et al. (1994), which Mitrofanov et al. show to be a consequence of the selection criterion use by Norris et al.. Mitrofanov et al. report on several measures of burst duration. In the first, bursts with peak fluxes  $< 1 \text{ cm}^{-2} \text{ s}^{-1}$  are compared to bursts with peak flux  $> 1 \text{ cm}^{-2} \text{ s}^{-1}$ . The total widths of the averaged light profiles are  $6.57 \pm 0.09 \text{ s}$  and  $6.64 \pm 0.1 \text{ s}$  respectively. This implies a duration ratio of  $0.99 \pm 0.13$ . In comparison, one finds a time-dilation ratio of 1.22 for a monoluminous model with a width energy dependence of  $\nu^{-0.23}$ , and a time-dilation ratio of 1.12 for a power-law luminosity model with the same energy dependence. The data is two standard deviations from the first, but it is only one standard deviation from the second. In

the second, bursts with peak fluxes  $< 0.45 \text{ cm}^{-2} \text{ s}^{-1}$  are compared to bursts with peak flux  $> 2.5 \text{ cm}^{-2} \text{ s}^{-1}$ . These bursts give total widths of  $6.50 \pm 0.13 \text{ s}$  and  $6.21 \pm 0.15 \text{ s}$  respectively. The duration ratio is then  $1.05 \pm 0.20$ . Taking  $0.45 \text{ cm}^{-2} \text{ s}^{-1}$  for the low flux, one finds 1.49 for the monoluminous models and 1.27 for the power-law luminosity model. This data is a little over two standard deviations from the first model value and one standard deviation from the second model value. From this, one sees that the data can be considered consistent with a cosmological time dilation if bursts have a broad luminosity distribution function.

One study attempted to find a correlation between the peak flux and  $E_{peak}$ , the observed photon energy at which the  $\nu F_\nu$  curve has a maximum (Mallozzi et al. 1995). The advantages of using  $E_{peak}$  rather than burst timescale are that  $E_{peak}$  is strictly proportional to  $1/(1+z)$ , and its value varies by less than a factor of 10, whereas the duration is energy dependent, and it varies in value by several orders of magnitude. The study found that the average value of  $E_{peak}$  increases with peak flux, which one expects from cosmological effects. But the implied redshift factor is large. The subset of BATSE gamma-ray bursts with  $T_{90} > 2 \text{ s}$  produces a ratio of average  $E_{peak}$  of  $2.45^{+0.25}_{-0.66}$  for bursts with peak fluxes between  $5.90 \text{ cm}^{-2} \text{ s}^{-1}$  and  $105.0 \text{ cm}^{-2} \text{ s}^{-1}$  relative to bursts with peak fluxes between  $0.95 \text{ cm}^{-2} \text{ s}^{-1}$  and  $1.30 \text{ cm}^{-2} \text{ s}^{-1}$ . In contrast, model calculations for the parameters given above produce 1.61 for the monoluminous model and 1.30 for the power law luminosity model, which are 1.3 and 1.7 standard deviations from the data. For a lower peak flux range of  $0.95 \text{ cm}^{-2} \text{ s}^{-1}$  to  $1.30 \text{ cm}^{-2} \text{ s}^{-1}$ , the ratio is  $1.99^{+0.36}_{-0.38}$ , while the models give 1.47 and 1.23 for the monoluminous and the power law luminosity cases, which are 1.4 and 2.0 standard deviations from the data.

Taken individually, the tests that show a correlation of burst duration or characteristic spectral energy with peak flux are consistent with the models, but taken together, they are inconsistent, because all of these tests are systematically above the monoluminous model by one standard deviation and above the power-law luminosity model by two standard deviations. The reported correlations are therefore inconsistent with the theoretical models presented in this article. In conclusion, the reported correlations must be a consequence of an intrinsic correlation of  $E_{peak}$  and burst duration with peak flux. No cosmological model can simultaneously fit the observed flux distribution and the claimed time dilation and redshift ratios, and no cosmological model with a power-law luminosity distribution can fit the claimed time dilation and redshift ratios for any value of  $F_0$ .

## 7. The Flux Distribution for Redshift-Selected Subsets

The observations require an intrinsic correlation of  $E_{peak}$  and time dilation with luminosity. The question is whether a direct measure of this correlation exists. The recent studies of the flux distribution of gamma-ray bursts selected by hardness ratio presents such an opportunity.

The discussion that follows depends on the two critical assumptions underlying equation (8). First, for  $z \ll 1$ ,  $n_0(\tau)$  is a constant. Second, the gamma-ray burst characteristics must be independent of  $\tau$ , particularly for  $z \ll 1$ . These assumptions are reasonable given that the observed flux distribution goes to a power-law of index  $-5/2$  for large flux, which is a natural consequence of these assumptions.

The discussion in §3 and §4 shows that the power-law index of the flux distribution deviates from  $-5/2$  at  $F_0$ . This flux is dependent on the spectral parameters through  $\mathcal{F}(L, \vec{p})$  in the  $L$  argument of  $\Phi(L, \vec{p})$ , but this dependence is weak, as demonstrated by the values for  $F_0$  derived from model fits and given in Tables 3 and 4. If there is a strong dependence of  $F_0$  on spectral parameter, it can only enter through the direct dependence of the distribution function  $\Phi(L, \vec{p})$  on the spectral parameter  $\vec{p}$ . In this case,  $L_0$  is a function of  $\vec{p}$ , which makes  $F_0$  a function of  $\vec{p}$  through equation (6).

The dependence of  $F_0$  on  $L$  is graphically demonstrated in Figure 11, where  $E_{peak}$  is plotted as a function of flux for specific values of  $L$  and  $E_p$ , where  $E_p$  is the value of  $E_{peak}$  when  $z = 0$ . The solid curves give the variation of  $E_{peak}$  with  $F$  when  $E_p$  decreases with  $L$ , the dotted curves give  $E_{peak}$  for different values of  $L$  and the same  $E_p$ , and the dashed curves give  $E_{peak}$  for different values of  $E_p$  and the same  $L$ . In these curves,  $z \ll 1$  when  $E_{peak}$  is constant with  $F$ , so the flux distribution for a given  $E_{peak}$  is a power law of index  $-5/2$ . Regarding these sets of curves as three models of the dependence of  $L_0$  on  $E_p$ , one sees that when  $E_p$  decreases with  $L_0$ , the value of  $F_0$  for bursts selected by  $E_{peak}$  decreases with  $E_p$ . The solid curves exhibit a second property not yet touched upon—the crossing of curves. This means that bursts with a given  $F$  and  $E_{peak}$  can have a variety of values for  $L$  and  $z$ .

For the spectral model in §2, the selection of bursts by  $E_{peak}$  is equivalent to turning the spectral parameter  $\Psi$  into a function of  $E_p$  and  $z$ . Equation (8) becomes

$$\frac{dN}{dt d\Omega dF dz dE_{peak} d\tau_T} = n_0[\tau(z)] \Phi \left\{ \frac{F}{\mathcal{F}(z)}, \Psi[E_{peak}(1+z), \tau_T] \right\} \mathcal{F}(z)^{-1} \cdot \frac{r^2}{(1+z)\sqrt{1+2q_0z}} \left| \frac{d\Psi(E_p)}{dE_p} \right|_{E_{peak}(1+z)}. \quad (22)$$

The function  $\Psi(E_p)$  is given by  $\Psi(E_p) = \sigma'_c(E_p/mc^2) E_p/\sigma_T mc^2$ , where  $\sigma_c$  is the

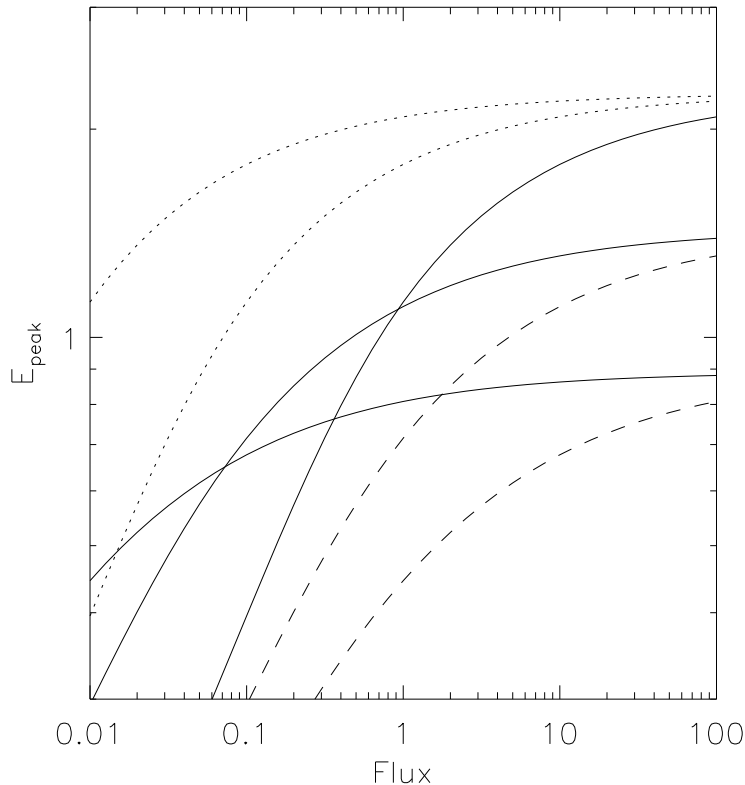


**Fig. 11**—Models of  $E_{peak}$  versus  $F$  for constant  $L$ . From top to bottom, the solid lines are for  $\Psi = -0.12$  and  $F_0 = 1$ ,  $\Psi = -0.14$  and  $F_0 = 0.1$ , and  $\Psi = -0.16$  and  $F_0 = 0.01$ . From top to bottom, the dotted lines are for  $F_0 = 0.01$  and  $F_0 = 0.1$  with  $\Psi = -0.12$ . From top to bottom, the dashed lines are for  $\Psi = -0.14$  and  $-0.16$  with  $F_0 = 1$  and  $F_0 = 0.1$ . The flux is measured in the 50 keV to 300 keV energy band.

Klein-Nishina cross section and the prime represents the first derivative with respect to  $E_p/mc^2$ . For  $E_p/mc^2 \gg 0.1972$ ,  $\Psi(E_p) \approx [\log(2E_p/mc^2) - 1/2]mc^2/E_p$ , so the first derivative of  $\Psi(E_p)$  is  $d\Psi(E_p)/dE_p = [\log(2E_p/mc^2) - 3/2]mc^2/E_p^2$ . Therefore, the derivative term does not dramatically change the dependence of equation (22) on  $z$  from that in equation (8). The important difference from equation (8) is the dependence of  $\Phi$  on  $E_{peak}(1+z)$  in equation (22). The observed distribution of  $E_{peak}$  in the BATSE catalog falls rapidly to zero for  $300 \text{ keV} < E_{peak} < 1 \text{ MeV}$  (Mallozzi et al. 1995). Because the  $E_{peak}$  distribution is narrow,  $\Phi(L, \vec{p})$  must fall rapidly as  $E_p$  goes to infinity. This means that an additional upper limit on the value of  $z$  is set by the value of  $E_{peak}(1+z)$  at which the integrand no longer contributes significantly to the integral. When the integrand peak occurs at  $z_0 \ll 1$ , the maximum value of  $z$  is set by the dependence of  $\Phi$  on  $L$ , but when the peak occurs at  $z_0 \gg 1$ , the maximum value of  $z$  is set by the dependence on  $E_p$ . In the second case, the upper limit on  $z$  is independent of  $F$ . This limit sets an upper limit on  $L$  through the ratio  $F/\mathcal{F}(z, \vec{p})$ ; as  $F$  decreases, the upper limit on  $L$  decreases.

These results explain the results of recent studies (Pizzichini 1994; Belli 1995; Kouveliotou et al. 1996; Pendleton et al. 1997) of the BATSE flux distribution for gamma-ray bursts selected by hardness ratio. The hardness ratio is a measure of the



spectral shape, and it is dependent on the cosmological redshift because of the curvature in gamma-ray burst spectra below 1 MeV. It is therefore a proxy measure of  $E_{peak}$ . These studies show that the soft gamma-ray bursts have a flux distribution that is a power law of index  $-5/2$ . The hard gamma-ray bursts, however, follow a curve that falls below a  $-5/2$  power law. This is the behavior expected when  $E_p$  rises with luminosity.

The study of the burst distribution on the  $E_{peak}$ - $\log F$  plane may yield the luminosity distribution of gamma-ray bursts as a function of  $E_p$ . This would enable one to separate the intrinsic correlation of  $E_p$  with luminosity from the cosmological redshift. The way one approaches this problem is to select the group of burst with the highest value of  $E_{peak}$ . As one goes to lower flux for such bursts, the brighter bursts redshifted out of the  $E_{peak}$  range being examined, and no bursts enter this band through a redshift from a higher value of  $E_{peak}$ . As a consequence, the peak-flux distribution deviates from the  $-5/2$  power law in a manner determined by the luminosity distribution function for  $E_p = E_{peak}$ , and a luminosity distribution function for this value of  $E_p$  can be derived. One can then subtract from the density of bursts with smaller values of  $E_{peak}$  the density of bursts with large values of  $E_p$  that are strongly redshifted. One then selects bursts with a lower value of  $E_{peak}$  to repeat the process. The uncertainty in the feasibility of this analysis is in whether the BATSE data set is of sufficient size and quality to perform such a test.

## 8. Summary of Major Points

A monoluminous burst distribution produces good fits to the BATSE peak-flux distribution for very specific spectral parameters. The parameters that produce the best values of  $\chi^2$  are themselves strongly dependent on the value of  $q_0$ . The spectra that are nearly power laws do not produce good fits: a curved spectrum is required to reproduce the observations. The spectral parameters derived from fits to gamma-ray burst spectra produce peak-flux distributions that fit the observed distribution well. From model fits to the peak-flux distribution, one finds that gamma-ray bursts at  $z = 1$  have peak fluxes of  $\approx 1\text{--}2 \text{ cm}^{-2} \text{ s}^{-1}$  for  $q_0 = 0.5$  and  $\approx 2.5\text{--}4 \text{ cm}^{-2} \text{ s}^{-1}$  for  $q_0 = 0.1$ . I confirm the conclusion that the  $q_0 = 0.5$  cosmology cannot simultaneously reproduce the observed flux distribution and the reported time dilation–burst flux correlations (Fenimore & Bloom 1995), and I find that the  $q_0 \ll 0.5$  cosmology can never reproduce the observed time dilation–burst flux correlation, independent of the fit to the peak flux distribution.

When gamma-ray bursts have a distribution of luminosities, the shape of the low end of the peak-flux distribution can be determined by the shape of the luminosity distribution (Mészáros & Mészáros 1995). If the luminosity distribution below some value is proportional

to  $L^{-\beta}$ , then the asymptotic flux distribution as  $F \rightarrow 0$  is  $\propto F^{-\beta}$  when  $\beta \gtrsim 0.6$  for  $q_0 = 0.5$  and  $\beta \gtrsim 1.15$  for  $q_0 = 0.1$  when there is only mild source density evolution. The precise values on the right side of these inequalities are dependent on the burst spectrum and the density evolution of burst sources. When the inequalities are violated, the peak-flux distribution is that found for monoluminous models. Equations (12) and (16) give these limits and their dependence on source density evolution. The luminosity distribution can formally diverge as the luminosity goes to 0; below a critical luminosity, which is set by the peak-flux threshold of the observing instrument, the luminosity distribution no longer contributes to the peak-flux distribution. A power-law luminosity distribution  $\propto L^{-\beta}$  with an upper cutoff at  $L_0$  produces peak-flux distributions that fit the BATSE 3B data well for most spectral parameters. One finds that  $\beta \approx 1.5$ . This shows that the luminosity distribution need not be a standard candle or a steep power law to produce a good fit to the data.

When the power-law luminosity distribution defines the shape of the flux distribution, so that  $\beta \approx 1.5$ , the gamma-ray bursts at a given peak flux have a distribution of redshifts that is strongly peaked at  $z < 1$ . As  $\beta$  becomes smaller, the peak in the  $z$  distribution goes to infinity, and the distribution rises monotonically. The distribution goes to zero at some maximum value for  $z$  that is set by the peak flux. When  $\beta \approx 1.5$ , the average redshift is a weak function of peak flux when the peak flux is small. At the peak-flux threshold of BATSE, the maximum redshift that a burst can have is  $\gtrsim 3$ , while the average redshift at threshold is  $< 1$ . From the model fits to the peak flux distribution, the distribution in  $z$  has an upper limit of  $z = 1$  when  $F_0 \gtrsim 5 \text{ cm}^{-2} \text{ s}^{-1}$ , although this limit on  $F_0$  is poorly constrained. This implies that the most luminous gamma-ray bursts have an isotropic luminosity of  $\gtrsim 2 \times 10^{51} \text{ ergs s}^{-1}$  in the 50 keV to 300 keV energy band for  $H_0 = 75 \text{ km s}^{-1} \text{ Mpc}^{-1}$ . For a burst duration of 10 s, the fluence is  $\gtrsim 2 \times 10^{52} \text{ ergs s}^{-1}$ , making solar mass objects implausible sources of gamma-ray bursts.

A distinction in the literature is often made between narrow and broad luminosity distributions. By narrow, many authors mean either that the bursts are nearly monoluminous, which is a statement about the burst physics, or that a high percentage of observed bursts have nearly the same flux, which is a statement about the detector threshold. A more useful distinction is between luminosity-dominated flux distributions and density-dominated flux distributions. In the former, the shape of the flux distribution is determined by the shape of the luminosity distribution, and the average redshift, which is weakly dependent on peak flux, is  $\approx 1$ . In the latter, the shape of the peak-flux distribution is determined by the spatial distribution of gamma-ray bursts, and there is nearly a one-to-one correspondence between redshift and peak flux.

The large errors in the model parameters do not strongly constrain the distribution in  $z$  at a given peak flux. Because of this, large values of  $z$  found from model fits of the Compton attenuation spectrum to BATSE gamma-ray bursts are consistent with the values of  $z$  possible in the flux distribution produced by a cosmological model with a luminosity distribution function.

Because one averages over the distribution in  $z$  when calculating the average burst duration and the characteristic photon energy at a given peak flux, the average time dilation factor does not equal the average redshift factor; the former is larger than the latter. From the model fits to the observed peak-flux distribution, one expects bursts with two different values of peak flux, one 10 times the other, to have ratios of average time dilations and ratios of average spectral redshifts of  $< 1.6$ . Independent of the best fit to the flux distribution, the maximum possible time dilation and redshift ratios are  $< 1.7$ . The reported correlations of  $E_{peak}$  and burst time scale with peak flux are much larger than this by 1.5 to 2 standard deviations, so they are not consequences of cosmological expansion in the models examined above. Within this model, only the addition of an intrinsic correlation with luminosity can create the observed correlations. An alternative not explored in this article is strong source evolution, with  $\alpha \approx 3$  (Reichart & Mészáros 1997). From equations (12) and (16), the flux distribution in this case is density-dominated. On the other hand, since cosmological expansion produces a modest effect when a luminosity distribution determines the peak flux distribution, the absence of a correlation cannot be taken as evidence that gamma-ray bursts are not cosmological.

The presence of an intrinsic correlation of  $E_{peak}$  with flux may be tested by examining the flux distribution for bursts with different values of  $E_{peak}$ , the energy at which the  $\nu F_\nu$  curve has a maximum. If the intrinsic value of  $E_{peak}$  decreases with luminosity, then the bursts with the smallest observed values of  $E_{peak}$  will have a peak-flux distribution that falls away from a  $-5/2$  power law at a lower value of  $F$  than do the bursts with a high value of  $E_{peak}$ . This is observed when gamma-ray bursts are selected by hardness ratio, which is a proxy for  $E_{peak}$ .

One justification given for more sensitive gamma-ray burst detectors is the measurement of the gamma-ray burst flux distribution at fluxes below the thresholds of current gamma-ray experiments. If gamma-ray bursts are at cosmological redshifts of  $z \approx 1$ , then such an effort is of limited value, because the behavior of the distribution is strongly model dependent, and is easily modeled by a luminosity distribution function. Of more value are large numbers of gamma-ray bursts with well characterized spectra. Such burst catalogs allow one to discern the dependence of burst luminosity on spectral parameters, which then allows one to disentangle the intrinsic correlation of burst luminosity with  $E_{peak}$  from the

correlation from the cosmological expansion. It is this that justifies accumulating as large a data set as possible, and underlies the value of continued observations by the BATSE.

## REFERENCES

- Belli, B. M. 1995, *Ap&SS*, 231, 43
- Brainerd, J. J. 1992, *Nature*, 355, 522
- Brainerd, J. J. 1994a, *ApJ*, 428, L1
- Brainerd, J. J. 1994b, *ApJ*, 428, 21
- Brainerd, J. J., Preece, R. D., Briggs, M. S., Pendleton, G. N., & Paciesas, W. S. 1996a, in *AIP Conf. Proc. 384, Gamma-Ray Bursts*, ed. C. Kouveliotou, M. S. Briggs, & G. J. Fishman (New York: AIP), 148
- Brainerd, J. J., Preece, R. D., Briggs, M. S., Pendleton, G. N., & Paciesas, W. S. 1996b, *ApJ*, submitted
- Cohen, E., & Piran, T. 1995, *ApJ*, 444, 25
- Davis, S. P., Norris, J. P., Kouveliotou, C., Fishman, G. J., Meegan, C. A., & Paciesas, W. S. 1994, in *Gamma-Ray Bursts*, ed. G. J. Fishman, J. J. Brainerd, & K. Hurley (AIP: New York), 182
- Emslie, A. G., & Horack, J. M. 1994, *ApJ*, 435, 16
- Fenimore, E. E., Epstein, R. I., Ho, C., Klebesadel, R. W., Lacey, C., Laros, J. G., Meier, M., Strohmayer, T., Pendleton, G., Fishman, G., Kouveliotou, C., & Meegan, C. 1993, *Nature*, 366, 40
- Fenimore, E. E., & Bloom, J. S. 1995, *ApJ*, 453, 25
- Groot et al. 1997, *IAU Circ.*, 6584
- Hakkila, J., Meegan, C. A., Pendleton, G. N., Horack, J. M., Briggs, M. S., Paciesas, W. S., & Emslie, A. G. 1995, *ApJ*, 454, 134
- Hakkila, J., Meegan, C. A., Horack, J. M., Pendleton, G. N., Briggs, M. S., Mallozzi, R. S., Koshut, T. M., Preece, R. D., & Paciesas, W. S. 1996, in *Proceedings of the Third Huntsville Gamma-Ray Burst Symposium*, ed. C. Kouveliotou, M. S. Briggs, & G. J. Fishman (New York: AIP), 387
- Horack, J. M., Emslie, A. G., & Hartmann, D. H. 1995, *ApJ*, 447, 474
- Hueter, G. J., 1984, in *AIP Conf. Proc. 115, High-Energy Transients in Astrophysics*, ed. S. E. Woosley (New York: AIP), 373

- Kouveliotou, C., Koshut, T., Briggs, M. S., Pendleton, G. N., Meegan, C. A., Fishman, G. J., & Lestrade, J. P. 1996, in Proceedings of the Third Huntsville Gamma-Ray Burst Symposium, ed. C. Kouveliotou, M. S. Briggs, & G. J. Fishman (New York: AIP), 42
- Lee, T. T., & Petrosian, V. 1996, *ApJ*, 474, 37
- Mallozzi, R. S., Paciasas, W. S., Pendleton, G. N., Briggs, M. S., Preece, R. D., Meegan, C. A., & Fishman, G. J. 1995, *ApJ*, 454, 597
- Mallozzi, R. S., Pendleton, G. N., & Paciasas, W. S. 1996, *ApJ*, 471, 636
- Matz, S. M., Forrest, D. J., Vestrand, W. T., Chupp, E. L., Share, G. H., & Rieger, E. 1985, *ApJ*, 288, L37
- Mészáros, P., & Mészáros, A. 1995, *ApJ*, 449, 9
- Metzger, A. E., Parker, R. H., Gilman, D., Peterson, L. E., & Trombka, J. I. 1974, *ApJ*, 194, L19
- Mitrofanov, I. G., Kozlenkov, A. A., Chernenko, A. M., Dolidze, V. Sh., Pozanenko, A. S., Ushakov, D. A., Atteia, J.-L., Barat, C., Niel, M., & Vedrenne, G. 1993, in AIP Conf. Proc. 280, Compton Gamma-Ray Observatory, ed. M. Friedlander, N. Gehrels, & D. J. Macomb (New York: AIP), 761
- Mitrofanov, I. G., Chernenko, A. M., Pozanenko, A. S., Paciasas, W. S., Kouveliotou, C., Meegan, C. A., Fishman, G. J., & Sagdeev, R. Z. 1994, in AIP Conf. Proc. 307, Gamma-Ray Bursts, ed. G. J. Fishman, J. J. Brainerd, & K. Hurley (New York: AIP), 187
- Mitrofanov, I. G., Chernenko, A. M., Pozanenko, A. S., Briggs, M. S., Paciasas, W. S., Fishman, G. J., Meegan, C. A., & Sagdeev, R. Z. 1996, *ApJ*, 459, 570
- Nemiroff, R.J., Norris, J. P., Bonnell, J. T., Wickramasinghe, W. A. D. T., Kouveliotou, C., Paciasas, W. S., Fishman, G. J., & Meegan, C. A. 1994, *ApJ*, 435, L113
- Norris, J. P., Nemiroff, R. J., Scargle, J. D., Kouveliotou, C., Fishman, G. J., Meegan, C. A., Paciasas, W. S., & Bonnell, J. T. 1994, *ApJ*, 424, 540
- Norris, J. P., Bonnell, J. T., Nemiroff, R. J., & Scargle, J. D. 1996, in AIP Conf. Proc. 384, Gamma-Ray Bursts, ed. C. Kouveliotou, M. S. Briggs, & G. J. Fishman (New York: AIP), 77
- Pendleton, G. N., Mallozzi, R. S., Paciasas, W. S., Briggs, M. S., Preece, R. D., Koshut, T. M., Horack, J. M., Meegan, C. A., Fishman, G. J., Hakkila, J., & Kouveliotou, C. 1996, *ApJ*, 464, 606
- Pendleton, G. N., et al. 1997, in preparation.

- Petrosian, V., & Lee, T. T. 1996, *ApJ*, 467, L29–L32
- Pizzichini, G. 1994, unpublished
- Preece, R. D., Briggs, M. S., Pendleton, G. N., Paciasas, W. S., Matteson, J. L., Band, D. L., Skelton, R. T., & Meegan, C. A. 1996, *ApJ*, 473, 310
- Reichart, D. E., & Mészáros, P. 1997, *ApJ*, in press
- Rutledge, R. E., Hui, L., & Lewin, W. H. G. 1995, *MNRAS*, 276, 753
- Ulmer, A., & Wijers, R. A. M. J. 1995, *ApJ*, 439, 303
- Ulmer, A., Wijers, R. A. M. J., & Fenimore, E. E. 1995, *ApJ*, 440, L9
- Weinberg, S. 1972, *Gravitation and Cosmology: Principles and Applications of the General Theory of Relativity*, (New York: Wiley)
- Wickramasinghe, W. A. D. T., Nemiroff, R. J., Norris, J. P., Kouveliotou, C., Fishman, G. J., Meegan, C. A., Wilson, R. B., & Paciasas, W. S. 1993, *ApJ*, 411, L55
- Wijers, R. A. M. J., & Paczyński, B. 1994, *ApJ*, 437, L107
- Yi, I. 1994, *ApJ*, 431, 543